JOURNAL OF PROPULSION AND POWER
Vol. 25, No. 3, May–June 2009

Investigation of Self-Sustaining Waves in Metastable Systems: Deflagration-to-Detonation Transition

N. N. Smirnov,* V. F. Nikitin,† and S. Alyari Shurekhdeli‡
Lomonosov Moscow State University, 119992, Moscow, Russia

DOI: 10.2514/1.33078

Self-sustaining waves can propagate in metastable media; energy needed to support such waves is released by the wave itself. The examples are waves of combustion and waves of boiling in overheated liquids. As a rule, two regimes of propagation exist: subsonic and supersonic. The difference is based on the different mechanisms of medium activation. Processes of transition between those regimes were less studied up to now, in comparison with pure subsonic or supersonic modes. Knowing mechanisms of controlling detonation initiation is important to work out effective preventive measures, such as suppressing deflagration-to-detonation transition in the case of combustible mixture ignition, and mitigation of a detonation wave in case it is already developed. On the other hand, the advantages of burning fuel in a detonation regime in comparison with slow burning at constant pressure attract increasing attention to pulse detonation burning chambers and to their possible application to new generation engines. The deflagration-to-detonation transition can be a principal stage of the work cycle in a pulse detonation engine, and the knowledge of details of this process and means of control can significantly decrease the predetonation distance and optimize the device. This work contains a review of the results obtained in theoretical and experimental investigations of deflagration-to-detonation transition processes in gases. Influence of internal geometry and flow turbulization on the detonation onset is considered; the influence of temperature and fuel concentration in the unburned mixture is discussed. Transitional processes of overheated liquid boiling up are also analyzed.

Nomenclature

A_r	=	Arrhenius preexponential factor for reaction r
a_p	=	sound velocity in reaction products at constant pressure
C_{fuel}	=	fuel volume concentration in the mixture
C_{N_2}	=	nitrogen volume concentration in the mixture
C_μ, $C_{1\varepsilon}$, $C_{2\varepsilon}$, and C_g	=	turbulence model constants
$\hat{c}_p$	=	specific heat capacity of gas mixture at constant pressure
D	=	overall laminar diffusion coefficient
D_θ	=	dissipation of mean squared temperature deviation
E	=	total (internal and kinetic) energy of fluid
$\dot{E}_{\text{ex}}$	=	energy flux from ignition by the outer source
E_{ig}	=	ignition energy
e_{ig}	=	ignition energy per mass unit
e_k	=	specific internal energy of component k
G_k^0	=	Gibbs specific energy of component k at reference pressure
h_k	=	specific enthalpy of gas component k
$\mathbf{I}$	=	identity tensor
$\mathbf{J}_k$	=	turbulent diffusive flux to component k
K_r	=	equilibrium constant of reaction r
k	=	specific energy of turbulence
k_{br}	=	backward rate of reaction r
k_f	=	turbulence energy at the reaction front
k_{fr}	=	forward rate of reaction r
k_0	=	initial specific energy of turbulence
L_b	=	length of a bridge connecting two chambers
L_c	=	length of a chamber of wider cross section
L_d	=	predetonation length
$\tilde{L}_d$	=	dimensionless predetonation length
l_{ref}	=	turbulence length scale
N_c	=	number of settling chambers
n_r	=	degree factor for chemical reaction r
P_θ	=	production of mean squared temperature deviate due to mixing
p	=	pressure
p_{atm}	=	standard atmosphere pressure
p_{ref}	=	pressure scale
p_0	=	initial pressure
Q_{ig}	=	heat flux from the ignition source
$\mathbf{q}$	=	turbulent energy flux
$\mathbf{q}^c$	=	turbulent conductive heat flux
R	=	radius of the cylindrical vessel
R_g	=	universal gas constant
R_{ref}	=	Clapeyron gas constant
Re	=	Reynolds number
r	=	radial coordinate in cylindrical coordinate system
S_u	=	laminar velocity of combustion
Sr	=	Strouhal number
T	=	temperature of gas
T_{ar}	=	activation temperature for chemical reaction r
T_{ref}	=	temperature scale
T_0	=	initial temperature
T'	=	temperature disturbance
t	=	time
t_d	=	predetonation time
t_{ig}	=	time of ignition
t_{ref}	=	temperature scale
$\mathbf{u}$	=	fluid velocity vector

Received 26 June 2007; revision received 27 September 2008; accepted for publication 2 October 2008.

*Professor, Faculty of Mechanics and Mathematics; ebifsun1@mech.math.msu.su.

†Associate Professor, Faculty of Mechanics and Mathematics; vfnikster@gmail.com.

‡Ph.D. Student, Faculty of Mechanics and Mathematics; ebifsun1@mech.math.msu.su.

V_f	=	velocity of combustion or detonation front
V_{rms}	=	characteristic velocity of turbulence
v_{CJ}	=	Chapman–Jouguet velocity
W_θ	=	production of mean squared temperature deviation due to chemistry
W_k	=	molar mass of gas component k
x	=	axial coordinate in cylindrical coordinates system
x_{ref}	=	length scale
Y_k	=	mass fraction of gas component k
∂_t	=	partial derivative with respect to time
ε	=	turbulent energy decay rate
η	=	molecular viscosity of gas
η_{ref}	=	viscosity scale
η_0^t	=	initial eddy viscosity
θ	=	mean squared deviation for temperature
θ_m	=	limiting value for the mean squared temperature deviation
λ	=	laminar thermal conductivity of gas
ν'_{kr}, ν''_{kr}	=	stoichiometric coefficients (input, output) for component k in reaction r
ν^t	=	turbulent kinematic viscosity
ρ	=	gas density
ρ_{ref}	=	density scale
σ	=	ratio of gas density
σ_d, σ_t, and σ_ε	=	turbulence model constants
$\boldsymbol{\tau}$	=	turbulent stresses tensor
$\boldsymbol{\tau}^t$	=	Reynolds tensor term within turbulent stresses tensor
ϕ	=	ratio of actual fuel concentration in the mixture to a stoichiometric one
ω_{ij}	=	specific mass production rate of component i via chemical transformations in reaction j
$\dot{\omega}_k$	=	specific mass production rate of component k via chemical reactions in gas phase

I. Introduction

IN A broad sense, the regimes of deflagration and detonation indicate propagation of self-sustaining exothermal waves in a metastable medium, and the difference of mechanisms induces essential differences in the wave structure and propagation velocity. In a narrow sense, those regimes are waves of combustion and detonation in combustible mixtures, whereas the exothermicity is a consequence of heat release in chemical reactions. The waves of overheated liquid boiling up are also related to those regimes; accumulated heat energy is transformed there into the energy of compressed vapor.

An analysis of detonation initiation by local energy release reveals two different scenarios. The first scenario is realized if a sufficiently strong shock is formed in the gas, the temperature and pressure behind the shock wave increase, and activate chemical reactions. Energy release from those reactions sustains the wave velocity at the level of self-sustaining detonation velocity, that is, the wave does not decay and its velocity is independent of the initiation energy. This scenario of detonation initiation was investigated extensively; they are presented in the works [1–6] and in the further works by listed authors.

The second scenario of detonation initiation is realized if the shock wave formed owing to local heat release is not sufficiently intensive to activate the chemical reactions before it decays, though the heating in the energy-release spot is sufficient to activate chemical reactions. In this case, a deflagration wave propagates from the energy-release ("ignition") spot with a subsonic velocity relative to the moving unburned gas. In this wave, the mechanism of reaction activation in subsequent layers is heating due to heat transfer from burnt layers rather than the compression of the subsequent layers in a shock wave. The combustion wave propagating over the gas leads to acceleration and turbulization of the flow ahead of the front, which in turn increases the flame-propagation velocity. Compression waves ahead of the combustion front converge and form one or several shocks catching up to each other. As the result, either the flame-propagation velocity is stabilized (slow diffusive or fast turbulent), or detonation occurs with subsequent stabilization of the detonation velocity at the level of self-sustaining regime. Such a process of detonation initiation is called deflagration-to-detonation transition (DDT). In the present work, we will confine ourselves to considering these processes, namely, details of transition mechanisms and their sensitivity to changes in external governing parameters.

The study of DDT in hydrogen–air mixtures [7–10], and then in hydrocarbon–air mixtures [11,12] has shown that there are numerous DDT scenarios. Different mechanisms of the detonation initiation depend on a particular flow structure generated by the accelerating flame, and for this reason, all details of the DDT process cannot be reproduced in experiments. Currently, there are different viewpoints on the DDT mechanism: "explosion in an explosion" by Oppenheim and Urtiew [7] and gradient mechanism of "spontaneous combustion" by Zeldovich et al. [13]. Oppenheim and Urtiew observed spontaneous local explosions that were primary sources of the unburned gas layers compression, so that they "exploded" subsequently. Zeldovich et al. suggested the "spontaneous" mechanism according to which combustion wave velocity is determined by gradient of ignition induction time due to nonuniform heating of different unburned gas layers.

A subsequent theoretical analysis showed that a microscale increase in nonuniformity of the temperature distribution and an increase in concentration gradient near local exothermal centers ("hot spots") ahead of the flame front may turn out to be sufficient for an individual hot spot to develop either into a normal combustion wave, or to a detonation wave [14–19]. Oppenheim and Urtiew thought one needed a stochastic modeling of isolated hot spots because their origination and evolution was not understood at the time. However, subsequent modelers used entirely deterministic methods to identify the properties of hot spots and reasons for their origination. An analysis of theoretical and experimental results shows that self-ignition at one or several hot spots ahead of the accelerating flame with subsequent development of combustion or detonation wave from each local exothermal center is responsible for the existence of numerous DDT scenarios [20]. Shock waves arise owing to initiation and influence of the flame as an accelerating spherical piston. Reflection of compression waves from the container walls or from interfaces between gas mixtures of different densities leads to circulation of waves whose amplitude may increase owing to interaction with the flame [21–24]. The common feature of all these scenarios is the formation of local exothermal centers by Oppenheim and Urtiew's stochastic mechanism with the subsequent development of detonation at the microscale according to Zeldovich's spontaneous mechanism [17,20]. The first research of the DDT with the use of the Navier–Stokes model indirectly supports this effect [6]. The DDT study in the case of interaction of a reflected shock wave with the laminar flame [25,26] also shows that the deflagration-to-detonation transition at the hot spots follows the gradient mechanism, whereas the interaction between the shock wave and the combustion wave, as well as local inhomogeneities of the flow, creates conditions for the emergence of hot spots themselves.

The DDT can be promoted by inserting additional tripping devices into the channel, such as Shchelkin's spirals (Shchelkin and Troshin [27]), plates with orifices overlapping the cross section [28], or large-diameter settling chambers in the ignition section [11]. Flame propagation in channels of complicated geometry and in porous media was studied in the work by Abdullin et al [29]. The DDT was never observed in experiments in the free space, and such a transition was never realized in calculations, as far as the authors are aware.

The kinetics of chemical reactions also plays an important role in the DDT. It was first demonstrated [30] that, despite the common viewpoint, the ignition and combustion of hydrogen–air mixtures including situations at the atmosphere pressure near the third combustion limit occur almost exclusively by the branching-chain kinetic mechanism. The competition of reactions of chain branching and

chain termination together with self-heating determines the process kinetics as a whole. Adding a small amount of agent leading to chain termination can substantially inhibit the DDT.

Experimental studies of the DDT sensitivity to changes of the mixture parameters possess natural limitations on their accuracy, because the onset of numerous DDT regimes depends on stochastic flow inhomogeneities induced by the accelerating flame. Small changes of the flow parameters may lead to significant changes in the transition scenario. Besides, it is practically impossible to perform a change of an individual parameter in a physical test without influencing other problem parameters.

Numerical investigations of the DDT process give a unique possibility of the gradual parameters varying independently of each other in order to properly study their influence on the transition scenario details. In the next sections, results of theoretical and experimental studies of the DDT in premixed homogeneous gases will be presented. The sensitivity of the DDT to changes of governing parameters will be considered.

Investigations of another type of metastable media, overheated liquids [31,32], showed that two regimes of boiling up exist, namely, "slow" and "fast" waves. The structure of those waves was analyzed, and the propagation mechanism was described; bubbles atomization and subsequent rapid increase of the phase interface surface are significant features of the mechanism. It was shown that the slow boiling waves are similar to the waves of deflagration in gas, and the energy of fluid overheating is transformed into the energy of the expanding vapor–fluid mixture. The final state of the medium behind such a wave is characterized by a point on the lower branch of the Hugoniot pressure-volume diagram, whereas the Mikhelson ray is tangential to the Hugoniot equilibrium curve. This picture makes it possible to characterize a slow boiling wave as a rarefaction jump. The fast boiling waves are similar to the detonation waves in a combustible gas; however, they propagate at supersonic velocity relating to conditions both ahead and behind the wave (weak detonation mode). Numerical experiments showed that at the conditions of intense heating, a slow boiling wave propagating in an unstable liquid transforms into a fast boiling wave. The transition between the regimes is accompanied by a rapid pressure increase and by further propagation of the compression waves in both directions from the transition location.

The present activities are aimed to study details of transition between the two wave propagation regimes in a metastable media and the influence of governing parameters on the transition scenario taking combustible gas mixtures as an example.

II. Experimental Investigations of Transition Processes in Gases

Experimental studies of pulse regimes of detonation initiation in hydrocarbon–air mixtures were performed in a variable-chamber device shown in Fig. 1. Methylene cyclopropane was used as a fuel. The procedure and the equipment of these experiments are described in detail in the work of Smirnov et al. [20].

The influence of the test section geometry on the turbulent flame acceleration and detonation or deflagration development was studied using chambers whose volume was changeable from one test to another. The inner surface of the side walls of the chambers 1 and 2 (see Fig. 1) was threaded, which allowed the cylindrical inserts 3 and 4 to be screwed into the chambers and thus, the chamber volume to be changed. The mixture was ignited in the chamber 1 by an ignition spark plug 5. The gas flow caused by the combustion zone expansion was strongly turbulized due to the setup geometry; a ring vortex was induced in the chamber 2, and this subsequently accelerated the flame propagation between the chambers. An increase of pressure in both chambers closed the reverse valve 6, and expansion of the combustion products into a narrow tube 7 caused additional acceleration of the flame due to the piston effect, thus improving conditions of the DDT development. After the detonation wave passed the acceleration tube 7, the rarefaction wave propagated in the tube from the right to the left; it decreased pressure in the tube 7 and in the chambers 1 and 2. Subsequently, the valve 6 was open again, and the fresh mixture filled the setup displacing the combustion products; the mixture was forced into the test setup by a compressor. After total displacement of the combustion products, the mixture was ignited again; the pressure subsequently raised and closed the valve. Then, the initiation of detonation in the tube 7 took place and thus, the cycle repeated. The test setup worked in a periodic regime as a pulsed detonation waves generator using a hydrocarbon–air mixture. Each sequential ignition took place in a turbulized gaseous media due to the process of mixture insertion.

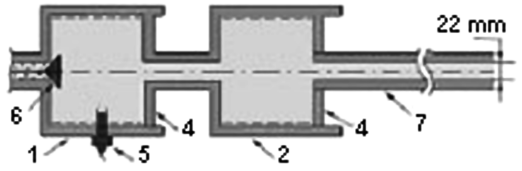

Fig. 1 Experimental device for DDT investigation in a tube, with two chambers of changeable volume.

Results of investigation showed that the predetonation length in a gasoline–air mixture in tubes 22 mm in diameter could be reduced to 1.5–2.0 m by using two settling chambers. The Schlieren photographs illustrating the multiplicity of transition scenario were published earlier [12,20,33]. Figure 2 shows the flow structure at various distances from the initiation section. The flame propagates from the left to the right; the time increases upward. Thus, the Schlieren photographs demonstrate the X–t diagram of the process. Here, the X axis corresponds to the coordinate along the test setup axis

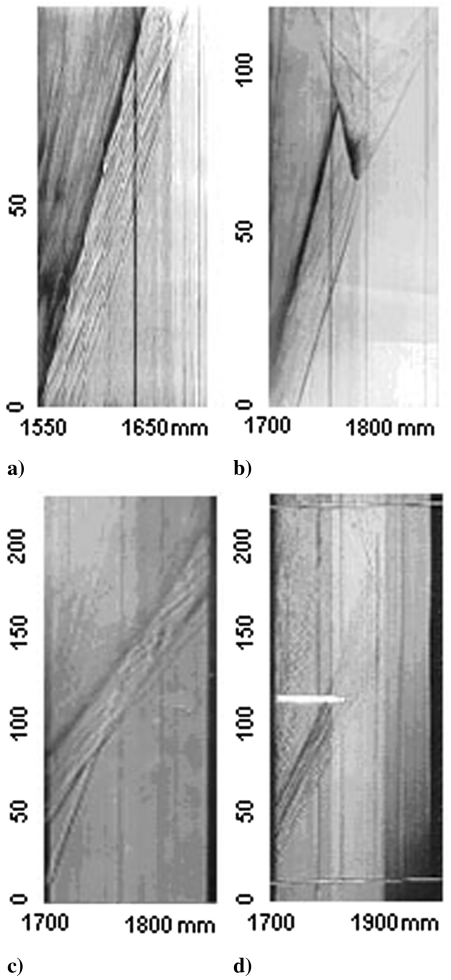

Fig. 2 a) Compression waves ahead of accelerating flame front; b) origin of detonation ahead of the turbulent flame, on a contact surface; c) self-ignition in a hot spot ahead of the flame front which gives birth to a new zone of combustion; d) self-ignition in several hot spots ahead of the flame front.

originating at the valve 6. The t axis is time originating at the beginning of photoregistration activation.

Figure 2a corresponds to the flow before the DDT. The settling chambers induce significant inhomogeneties in the flow upstream of the flame zone. The piston effect due to the expanding combustion products in the settling chambers generates a series of primary shock waves ahead of the flame front. Some waves are formed owing to interaction of transverse compression waves resulting from the turbulent flame acceleration. The flame propagates at the velocity up to 950 m/s in the laboratory frame of reference. Shocks originate behind the front, overtake it, and interact with the primary compression waves. Finally, their interaction brings to the formation a strong shock wave ahead of the flame front sustained by compression waves originated by the flame (Figs. 2b–2d). Because of relatively low intensity of the compression waves, they are not in contrast to the Schlieren pictures recording density gradients.

The detonation wave originates due to mixture ignition in the local exothermal centers (hot spots) ahead of the flame zone. The transition scenario illustrated by Fig. 2b is characterized by a hot spot in a high enthalpy zone on a contact interface originating after two primary shocks interaction. Figure 2c demonstrates the transition formed by a secondary combustion zone between the leading shock and the flame front due to a hot spot self-ignition. The combustion zone extends in all the directions from the hot spot, and in 180 μs the detonation wave is formed. Figure 2d illustrates the case where the ignition takes place sequentially in several hot spots ahead of the flame front. Each of those ignitions does not lead straightly to the formation of a detonation wave. The flame propagating from the hot spots first gives birth to volume combustion and then to the gas mixture compression behind the leading shock. The detonation wave originates in one of the exothermal centers near the shock wave, which is outside of the registration zone. The detonation formation is proved there by an existence of a retonation wave, propagating backward at 1350 m/s, which is seen in the upper part of Fig. 2d. The analysis of the experiments showed that the detonation wave formation takes place in one of the exothermal centers (hot spots) between the leading shock wave and the flame front. Dependent on the local flow structure and hot spots placement, the combustion may be brought either to detonation, or to deflagration propagating from one of the hot spots [20]. The initiation of detonation takes place under the condition that the temperature gradient is within the proper critical limits ensuring the necessary speed of spontaneous flame propagation [17,19].

Inhomogeneities in the compressed gas ahead of the flame front may take place, in particular, due to interaction of shock waves propagating upstream. Such a structure is formed when the ignition takes place at some distance from the closed end, and when the settling chambers generate an additional piston effect due to combustion products expansion. As seen from Fig. 2a, a series of compression waves is formed ahead of the flame front. Interaction of two shock waves, one catching the other, brings to formation one leading shock propagating in the same direction, a reflected centered rarefaction wave, and a contact surface between them, separating gases of different temperature and density.

Contact surfaces, as zones of high gradients of density, are well distinguished in the Schlieren photographs of Figs. 2b–2d. Hot spots ahead of the flame front, from which detonation (Fig. 2b) or deflagration (Fig. 2c) waves originate, appear after compressing the nonreacted gas by a sequence of compression waves. This process induces inhomogeneity of ignition delay times, a gas particle with the shortest ignition delay time exploding first. Those hot spots are developed directly on the contact surfaces, which are a result of interaction between leading shocks catching each other. The theoretical explanation of this phenomenon was done first in the work by Smirnov and Panfilov [34]. It was shown there that the self-ignition of the shock-compressed gas takes place in an individual exothermal center, which is characterized by minimal ignition delay time. The last depends on temperature of the mixture and physical time, elapsed as the gas was exposed to the elevated temperature. Ahead of the contact surface, the temperature of gas compressed by the bow shock is higher than the temperature behind the surface, where gas was twice compressed and then expanded adiabatically. The ignition induction time decreases with temperature increase. In the region between the bow shock and the contact surface, the gas mixture has the shortest induction time adjacent to the contact surface, because the gas is exposed here at the elevated temperature for the longest time. Therefore, the self-ignition takes place on the contact surface. Those conclusions are proven by results of direct numerical simulations [20,34].

After the gas is ignited in an exothermal center, gradients of temperature and concentrations established in the reaction zone determine the outcome of this event: detonation or deflagration wave [13]. In case of a detonation wave formation, the flow pictures are as shown in Figs. 2b and 2d. If a deflagration wave is developed and propagates from the ignition point with much lower velocity (Fig. 2c), ignition may also occur in the neighboring hot spots not yet reached by the wave (Fig. 2d).

III. Mathematical Model

The DDT processes were studied numerically on the basis of a system of equations derived from the Favre-averaged system of multispecies gas mixture dynamics equations of motion. A modified k–ε model of turbulence was used. The turbulence model is important for the DDT process modeling, due to its key role in the deflagration wave acceleration; on the other hand, after formation of the detonation wave, the influence of turbulence on its propagation is diminished. Temperature fluctuations influence the species production rates in chemical reactions. To model temperature fluctuations, the third equation was added to the system, which describes the dynamics of mean squared deviation of temperature [35]. Terms responsible for production and dissipation of this parameter, as well as the nonlinear terms responsible for chemical reactions rate, were modeled using the Gaussian integration method [36].

The system of governing equations for the averaged values of gas dynamic parameters is as follows:

$$\partial_t(\rho) + \nabla \cdot (\rho \mathbf{u}) = 0 \tag{1}$$

$$\partial_t(\rho Y_k) + \nabla \cdot (\rho \mathbf{u} Y_k) = -\nabla \cdot \mathbf{J}_k + \dot{\omega}_k \tag{2}$$

$$\partial_t(\rho \mathbf{u}) + \nabla \cdot (\rho \mathbf{u} \otimes \mathbf{u}) = -\nabla p + \nabla \cdot \boldsymbol{\tau} \tag{3}$$

$$\partial_t(\rho E) + \nabla \cdot (\rho \mathbf{u} E) = -\nabla \cdot p\mathbf{u} - \nabla \cdot \mathbf{q} + \nabla \cdot (\boldsymbol{\tau} \cdot \mathbf{u}) + \dot{E}_{\text{ex}} \tag{4}$$

Equations (1–4) include the continuity equation for the gas mixture in general, the mass balance equation of the kth species, and the momentum and energy equations for the mixture. The following expressions take place beside the equations:

$$\sum_k Y_k = 1, \qquad \sum_k \mathbf{J}_k = 0, \qquad \sum_k \dot{\omega}_k = 0$$

The state equation and the expression for total energy of the gas mixture are as follows:

$$p = R_g \rho T \sum_k Y_k / W_k, \qquad E = \sum_k Y_k e_k(T) + \mathbf{u} \cdot \mathbf{u}/2 + k$$

Turbulent heat flux in Eq. (4) is a sum of two terms: the conductive turbulent heat flux, and the energy transport due to turbulent diffusion,

$$\mathbf{q} = \mathbf{q}^c + \sum_k \mathbf{J}_k h_k(T)$$

Kinematic turbulent viscosity ν^t is determined within the frames of the k–ε turbulence model as $\nu^t = C_\mu k^2/\varepsilon$. For the turbulent fluxes, the following relations are used:

$$\boldsymbol{\tau} = (\eta + \rho\nu^t)(\nabla\mathbf{u} + \nabla\mathbf{u}^T - (2/3)(\nabla\cdot\mathbf{u})\mathbf{I}) - (2/3)\rho k\mathbf{I} \quad (5)$$

$$\mathbf{J}_k = -\rho(D + \nu^t/\sigma_d)\nabla Y_k, \qquad \mathbf{q}^c = -(\lambda + \rho\hat{c}_p\nu^t/\sigma_t)\nabla T \quad (6)$$

The rate of species generation in chemical reactions is denoted as $\dot{\omega}_k$. It is a sum of mass production rates ω_{kj} from all the reactions in the gas phase. The terms $\dot{\omega}_k$ are composed using exponential multipliers of the Arrhenius type. Therefore, they are sensitive to temperature fluctuations in a turbulent flow. Thus, temperature fluctuations should be incorporated into the model. We neglect influence of concentration fluctuations because the dependence is not so strong (polynomial). The temperature is considered hereafter as a stochastic function T with mean $\bar{T}$ and mean squared deviation $\theta = \overline{T'T'}$. To close the system of equations, two additional equations of the k–ε turbulence model are used determining the turbulence energy k and the energy dissipation rate ε, plus the third equation determining dynamics of temperature squared deviation $\theta = \overline{T'T'}$:

$$\partial_t(\rho k) + \nabla\cdot(\rho\mathbf{u}k) = \nabla\cdot((\eta + \rho\nu^t/\sigma_k)\nabla k) + \boldsymbol{\tau}^t\colon\nabla\mathbf{u} - \rho\varepsilon \quad (7)$$

$$\partial_t(\rho\varepsilon) + \nabla\cdot(\rho\mathbf{u}\varepsilon) = \nabla\cdot((\eta + \rho\nu^t/\sigma_\varepsilon)\nabla_\varepsilon) + (\varepsilon/k)(C_{1\varepsilon}\boldsymbol{\tau}^t\colon\nabla\mathbf{u} - C_{2\varepsilon}\rho\varepsilon) \quad (8)$$

$$\partial_t(\rho\hat{c}_p\theta) + \nabla\cdot(\rho\mathbf{u}\hat{c}_p\theta) = \nabla\cdot((\lambda + \rho\hat{c}_p\nu^t/\sigma_k)\nabla\theta) + P_\theta + W_\theta - D_\theta \quad (9)$$

Here, terms describing the production P_θ, W_θ, and the dissipation D_θ of squared temperature deviation θ are determined by the following formulas derived with the use of Favre averaging of the energy equation:

$$P_\theta = 2\rho\hat{c}_p\nu^t/\sigma_k(\nabla T)^2, \quad W_\theta = -\sum_k \overline{\dot{\omega}_k' T' h_k}, \quad D_\theta = C_g\rho\hat{c}_p\frac{\varepsilon}{k}\frac{\theta}{\theta_m - \theta} \quad (10)$$

The expression D_θ characterizing dissipation was obtained assuming the value $T = \bar{T} + T'$ is positive. Thus, a multiplier $1/(\theta_m - \theta)$ is introduced. The nonlinear Arrhenius law is used in the expression (10) determining the production of the temperature deviation in chemical processes W_θ. To calculate the terms $\overline{\dot{\omega}_k' T'}$, the Gaussian quadrature technique was used [36]:

$$\overline{T'A(T)} = \theta\frac{A(\bar{T} + \sqrt{3\theta}) - A(\bar{T} - \sqrt{3\theta})}{2\sqrt{3\theta}} \quad (11)$$

where $A(T)$ is a function incorporating an Arrhenius term or other complex nonlinearity. To estimate the limiting value θ_m, the following considerations are used. First, for normal distribution function, the probability of the deviation being twice more than the mean is less than 1%. Second, extensive experiments [37] were processed to determine the temperature deviation from the mean temperature value; it was observed that it stayed within one-half of the maximal averaged temperature. Therefore, we used the following estimate:

$$\theta_m = \bar{T}^2/4$$

We used standard k–ε turbulence model constants:

$$C_\mu = 0.09, \qquad C_{1\varepsilon} = 1.45, \qquad C_{2\varepsilon} = 1.92, \qquad \sigma_d = 1$$
$$\sigma_t = 0.9, \qquad \sigma_k = 1, \qquad \sigma_\varepsilon = 1.3$$

The constant C_g in Eq. (10) was determined on the basis of experimental data [37] as follows:

$$C_g = 2.8 \quad (12)$$

The production source term in Eq. (9) due to chemical reactions (10) acquires the form:

$$W_\theta - \overline{T'\sum_{j=1}\sum_{k=1} h_k\omega_{kj}} \quad (13)$$

Each term ω_{kj} contains an Arrhenius multiplier. To determine W_θ using the expression (13), one should calculate means $\overline{T'h_k(T)\omega_{kj}(T)}$ using the formula (11) and sum them up. The method of averaging nonlinear functions, as applied to this problem, was discussed in more detail in the work by Smirnov et al. [35].

Chemical interactions are modeled by a kinetic mechanism incorporating 12 gaseous species (both stable compounds and radicals) and 35 reversible reactions between them [38]. This mechanism is shown in Table 1.

For each chemical reaction, its direct rate is modeled using the Arrhenius law:

$$k_{fr} = A_r T^{n_r}\exp\left(-\frac{T_{ar}}{T}\right) \quad (14)$$

Coefficients used in Eq. (14) are shown in Table 1. Reverse reaction rates were obtained using minimal Gibbs energy principle:

$$k_{br}(T) = \frac{k_{fr}(T)}{K_r(T)}$$
$$K_r(T) = \exp\left(\frac{\sum_{k=1}^N(\nu''_{kr} - \nu'_{kr})G_k^0(T)}{R_gT}\right)\left(\frac{p_{\text{atm}}}{R_gT}\right)^{\sum_{k=1}^N(\nu''_{kr}-\nu'_{kr})}$$

Here, $p_{\text{atm}} = 1.01325\times10^5$ Pa is the standard atmosphere pressure, G_k^0 is a molar Gibbs energy of component k at the atmosphere pressure, and ν'_{kr} and ν''_{kr} are input and output stiocheometric coefficients of the species k in the reaction r, respectively.

Table 1 Kinetic mechanism for hydrogen–air mixture containing reactions with nitrogen. Units are mol, cm, s, and Kelvin

No.	Reaction	A_{fr}	n_r	T_{ar}
1	$H_2O + M \Leftrightarrow OH + H + M$	1.00×10^{24}	−2.2	59,000
2	$H_2 + M \Leftrightarrow 2H + M$	2.20×10^{14}	0.0	48,300
3	$O_2 + M \Leftrightarrow 2O + M$	2.60×10^{18}	0.0	59,580
4	$OH + M \Leftrightarrow H + O + M$	8.50×10^{18}	−1.0	50,830
5	$H_2 + O \Leftrightarrow OH + H$	1.80×10^{10}	1.0	4,480
6	$O_2 + H \Leftrightarrow OH + O$	2.20×10^{14}	0.0	8,455
7	$H_2O + O \Leftrightarrow 2OH$	5.80×10^{13}	0.0	9,059
8	$H_2O + H \Leftrightarrow OH + H_2$	8.40×10^{13}	0.0	10,116
9	$H_2 + O_2 \Leftrightarrow 2OH$	1.50×10^{15}	0.0	24,200
10	$N_2 + M \Leftrightarrow 2N + M$	3.70×10^{21}	−1.6	113,272
11	$NO + M \Leftrightarrow N + O + M$	5.25×10^{17}	−0.5	75,600
12	$O + N_2 \Leftrightarrow N + NO$	1.74×10^{14}	0.0	38,455
13	$O + NO \Leftrightarrow N + O_2$	1.51×10^{9}	1.0	19,439
14	$H + NO \Leftrightarrow N + OH$	1.70×10^{14}	0.0	24,500
15	$NO_2 + M \Leftrightarrow NO + O + M$	1.10×10^{16}	0.0	32,712
16	$OH + NO \Leftrightarrow H + NO_2$	2.00×10^{11}	0.5	15,500
17	$O_2 + NO \Leftrightarrow O + NO_2$	1.00×10^{12}	0.0	23,568
18	$NO_2 + N \Leftrightarrow 2NO$	3.60×10^{12}	0.0	0
19	$2NO_2 \Leftrightarrow 2NO + O_2$	2.00×10^{12}	0.0	13,500
20	$HO_2 + M \Leftrightarrow H + O_2 + M$	2.10×10^{15}	0.0	23,000
21	$H_2 + O_2 \Leftrightarrow H + HO_2$	1.90×10^{13}	0.0	24,100
22	$H_2O + O \Leftrightarrow H + HO_2$	4.76×10^{11}	0.375	28,743
23	$H_2O + O_2 \Leftrightarrow OH + HO_2$	1.50×10^{15}	0.5	36,600
24	$H_2O + OH \Leftrightarrow H_2 + HO_2$	7.90×10^{9}	0.43	36,100
25	$2OH \Leftrightarrow H + HO_2$	1.20×10^{13}	0.0	20,200
26	$OH + O_2 \Leftrightarrow O + HO_2$	1.30×10^{13}	0.0	28,200
27	$N + HO_2 \Leftrightarrow NO + OH$	1.30×10^{13}	0.0	1,000
28	$OH + NO_2 \Leftrightarrow NO + HO_2$	1.00×10^{11}	0.5	6,000
29	$H_2O_2 + M \Leftrightarrow 2OH + M$	1.20×10^{17}	0.0	22,900
30	$H + H_2O_2 \Leftrightarrow HO_2 + H_2$	1.70×10^{12}	0.0	1,900
31	$H + H_2O_2 \Leftrightarrow H_2O + OH$	5.00×10^{14}	0.0	5,000
32	$2HO_2 \Leftrightarrow H_2O_2 + O_2$	1.80×10^{13}	0.0	500
33	$HO_2 + H_2O \Leftrightarrow H_2O_2 + OH$	1.80×10^{13}	0.0	15,100
34	$OH + HO_2 \Leftrightarrow H_2O_2 + O$	5.20×10^{10}	0.5	10,600
35	$H_2O + O_2 \Leftrightarrow H_2O_2 + O$	3.40×10^{15}	0.5	44,800

Using the law of mass action, rates of species generation $\dot{\omega}_k$ are expressed as follows:

$$\dot{\omega}_k = W_k \sum_r (\nu''_{kr} - \nu'_{kr}) \left(k_{fr}(T) \prod_m \left(\frac{\rho Y_m}{W_m} \right)^{\nu'_{mr}} - k_{br}(T) \prod_m \left(\frac{\rho Y_m}{W_m} \right)^{\nu''_{mr}} \right) \tag{15}$$

The boundary conditions are set up on the walls and on the symmetry axis. The following assumptions are used: walls are thermally insulated with a noncatalytic, no-slip condition on the walls; and radial velocity and radial derivatives of axial velocity, temperature, and concentrations are zero on the symmetry axis

$$\text{wall}: u_x = u_r = 0, \qquad \frac{\partial T}{\partial n} = 0, \qquad \frac{\partial Y_k}{\partial n} = 0 \tag{16}$$

$$\text{axis}: u_r = 0, \qquad \frac{\partial u_x}{\partial r} = 0, \qquad \frac{\partial T}{\partial r} = 0, \qquad \frac{\partial Y_k}{\partial r} = 0 \tag{17}$$

The specific turbulent energy k is set to zero on the walls, and the von Neumann conditions are applied to the turbulence energy dissipation rate:

$$k = 0, \qquad \frac{\partial \varepsilon}{\partial n} = 0 \quad \text{at the wall}$$

Turbulence model coefficients C_μ, $C_{1\varepsilon}$, and $C_{2\varepsilon}$ are modified in the vicinity of the nearby wall using the Lam—Bremhorst law. All the standard turbulence model parameters and near-wall approximations were validated for nonreacting compressible turbulent flows [39]. The sensitivity of the solution to the turbulence model in general manifested for the regarded problem only on the stage of existence of a flame in a deflagration mode, which accelerated due to additional generation of turbulence ahead. After the detonation formation, wave propagation did not depend on the turbulent model, though a sharp increase of transfer coefficients sometimes brought additional losses in the reaction zone thus decreasing wave velocity. Initial values for turbulence and dissipation surpassing definite minimal values practically do not influence upon development of the process, because after the ignition, turbulence generated by the expanding combustion products surpasses the turbulence initial values and plays the key role in transport processes.

The ignition is modeled by the energy release from an external source within a spherical ball placed in the center of the first settling chamber. The temporal profile of the ignition energy source is taken as follows:

$$Q_{\text{ig}} = Q_{\text{ig}}(t) = \begin{cases} E_{\text{ig}}/t_{\text{ig}} & \text{at } t \le t_{\text{ig}} \\ 0 & \text{at } t \le t_{\text{ig}} \end{cases}$$

where Q_{ig} is a total heat flux from the source, E_{ig} is total ignition energy, and t_{ig} is the time of the ignition energy release. The zone of energy release is considered spherical with radius r_{ig} and volume Ω_{ig}. (For the tested structure, $r_{\text{ig}} = 1$ cm.) Energy flux per volume unit from an external source was $\dot{E}_{\text{ex}} = Q_{\text{ig}}/|\Omega_{\text{ig}}|$. The characteristic acoustic time of the volume was $t_{\text{ac}} = r_{\text{ig}}/a_p$. In further numerical simulations both cases of ignition time were shorter than acoustic time of the volume, and longer than what would be regarded.

IV. Numerical Algorithm and Model Testing

The system of governing equations being rewritten in a vector form was split into three parts relating to three different physical processes: chemistry source terms together with the generalized turbulence production and dissipation terms formed the "local part" of the equations. Convective terms formed the "hyperbolic part" of the equations; and turbulent viscous and transport terms formed the "parabolic part" of the equations

$$\frac{\partial U}{\partial t} + \frac{\partial}{\partial x}(F_x) + \frac{\partial}{\partial r}(rF_r) = H + P + S$$

where U is the vector of conservative variables, and F_x and F_r are the convective fluxes in the directions of respective coordinates. The source term on the right-hand part of the equation incorporates H as the hyperbolic part, P as the parabolic part, and S as the local part. The parts of the governing equations are shown in detail as follows:

$$U = \begin{bmatrix} \rho \\ \rho Y_1 \\ \rho Y_2 \\ \vdots \\ \rho Y_N \\ \rho u_x \\ \rho u_r \\ \rho E \\ \rho k \\ \rho \varepsilon \\ \rho \theta \end{bmatrix}, \qquad F_x = \begin{bmatrix} \rho u_x \\ \rho u_x Y_1 \\ \rho u_x Y_2 \\ \vdots \\ \rho u_x Y_N \\ \rho u_x u_x + p + 2/3\rho k \\ \rho u_x u_r \\ \rho u_x (E + p/\rho) + 2/3 \rho u_x k \\ \rho u_x k \\ \rho u_x \varepsilon \\ \rho u_x \theta \end{bmatrix}$$

$$F_r = \begin{bmatrix} \rho u_r \\ \rho u_r Y_1 \\ \rho u_r Y_2 \\ \vdots \\ \rho u_r Y_N \\ \rho u_x u_r \\ \rho u_r u_r + p + 2/3\rho k \\ \rho u_r (E + p/\rho) + 2/3 \rho u_r k \\ \rho u_r k \\ \rho u_r \varepsilon \\ \rho u_r \theta \end{bmatrix}$$

$$P = \begin{bmatrix} 0 \\ \frac{\partial}{\partial x}\left(D_i \frac{\partial Y_1}{\partial x}\right) + \frac{1}{r}\frac{\partial}{\partial r}\left(rD_i \frac{\partial Y_1}{\partial r}\right) \\ \frac{\partial}{\partial x}\left(D_i \frac{\partial Y_2}{\partial x}\right) + \frac{1}{r}\frac{\partial}{\partial r}\left(rD_i \frac{\partial Y_2}{\partial r}\right) \\ \vdots \\ \frac{\partial}{\partial x}\left(D_i \frac{\partial Y_N}{\partial x}\right) + \frac{1}{r}\frac{\partial}{\partial r}\left(rD_i \frac{\partial Y_N}{\partial r}\right) \\ 4/3\frac{\partial}{\partial x}\left(D_\mu \frac{\partial u_x}{\partial x}\right) - 2/3\frac{\partial}{\partial x}\left[D_\mu \frac{1}{r}\frac{\partial}{\partial r}(ru_r)\right] + \frac{1}{r}\frac{\partial}{\partial r}\left(rD_\mu \frac{\partial u_x}{\partial x}\right) + \frac{1}{r}\frac{\partial}{\partial r}\left(D_\mu \frac{\partial u_r}{\partial x}\right) \\ \frac{\partial}{\partial x}\left(D_\mu \frac{\partial u_r}{\partial x}\right) + \frac{\partial}{\partial x}\left(D_\mu \frac{\partial u_x}{\partial r}\right) + 4/3\frac{1}{r}\frac{\partial}{\partial r}\left(rD_\mu \frac{\partial u_r}{\partial x}\right) - 2/3\frac{u_r}{r}\frac{\partial D_\mu}{\partial r} - 4/3\frac{D_\mu u_r}{r^2} - 2/3\frac{\partial}{\partial r}\left(D_\mu \frac{\partial u_x}{\partial x}\right) \\ \frac{\partial}{\partial x}\left(D_T \frac{\partial T}{\partial x}\right) + \sum_{k=1}^{N} h_k \frac{\partial}{\partial x}\left(D_i \frac{\partial Y_k}{\partial x}\right) + \frac{\partial}{\partial x}(\tau_{xx}u_x + \tau_{xr}u_r) + \frac{1}{r}\frac{\partial}{\partial r}\left(rD_T \frac{\partial T}{\partial r}\right) + \sum_{k=1}^{N} h_k \frac{1}{r}\frac{\partial}{\partial r}\left(rD_i \frac{\partial Y_k}{\partial r}\right) + \frac{1}{r}\frac{\partial}{\partial x}[r(\tau_{xr}u_x + \tau_{rr}u_r)] \\ \frac{\partial}{\partial x}\left(D_k \frac{\partial k}{\partial x}\right) + \frac{1}{r}\frac{\partial}{\partial r}\left(rD_k \frac{\partial k}{\partial r}\right) \\ \frac{\partial}{\partial x}\left(D_\varepsilon \frac{\partial \varepsilon}{\partial x}\right) + \frac{1}{r}\frac{\partial}{\partial r}\left(rD_\varepsilon \frac{\partial \varepsilon}{\partial r}\right) \\ \frac{\partial}{\partial x}\left(D_T \frac{\partial \theta}{\partial x}\right) + \frac{1}{r}\frac{\partial}{\partial r}\left(rD_T \frac{\partial \theta}{\partial r}\right) \end{bmatrix}$$

$$H = \begin{bmatrix} 0 \\ 0 \\ 0 \\ \vdots \\ 0 \\ 0 \\ p/r \\ \dot{E}_{\text{ex}} \\ 0 \\ 0 \\ 0 \end{bmatrix}, \qquad S = \begin{bmatrix} 0 \\ \dot{\omega}_1 \\ \dot{\omega}_2 \\ \vdots \\ \dot{\omega}_N \\ 0 \\ 0 \\ 0 \\ \rho(C_\mu \frac{k^2}{\varepsilon} P_1 - kP_2 - \varepsilon) \\ \rho(C_{1\varepsilon} C_\mu k P_1 - C_{1\varepsilon}\varepsilon P_2 - C_{2\varepsilon}\frac{\varepsilon^2}{k} \\ P_\theta + W_\theta - D_\theta \end{bmatrix}$$

The local part was solved implicitly using an iterative algorithm independently for each grid node. The hyperbolic part was solved using explicit flux-corrected transport techniques [40]. The parabolic part was solved implicitly using 3-diagonal matrix solvers for linear equations [41]. This technique removes transport coefficients from the time step criterion and reduces it to the Courant—Friedrichs—Lewy (CFL) condition.

Splitting the system by coordinates was used according to MacCormack (as described by Anderson et al. [42]). The van Leer slope limiter [43,44] was used to improve the scheme approximation.

Validation of the numerical scheme was performed comparing the results of our tests with the exact gas-dynamics solutions and with model experiments on turbulent flame propagation in confined volumes. Additional verification was performed to estimate the influence of numerical viscosity and the slope limiter tool designed to improve the order of scheme accuracy on the turbulent viscosity behavior behind a shock wave.

Validation of the model was performed by comparing our numerical results with experimental and theoretical data on turbulent combustion velocity, predetonation length and predetonation time, and the Chapman–Jouguet (CJ) detonation velocity. In numerical simulations of processes in long tubes we used 20 cells for the radius and the necessary number along the tube axis with all cells having similar length and width; the time step was determined based on the CFL condition. The grid cell size was as chosen 1 mm based on the results of preliminary numerical simulations to guarantee that simulation results would not be influenced by further grid refinement.

The CJ detonation velocity v_{CJ} determined by means of 2-D calculations for various values of equivalency coefficient ϕ in hydrogen–air mixture was compared to the data published in the work [45] and to data obtained by 1-D calculation. The results of the comparison are shown in Fig. 3. The analysis of results shows that 2-D calculations yield underestimated values for detonation velocity compared, which can be attributed to friction-induced elevated dissipation of energy in the k–ε turbulence model, and to the transverse velocity components consuming part of the kinetic energy. Comparison of numerical results with experimental data helps to estimate uncertainty of the developed model: for lean mixtures errors do not exceed 5%, and for rich mixtures, 10%.

To test the numerical scheme describing turbulent reacting flow, calculations of turbulent combustion velocity for methyl spirit with oxygen enriched air were performed [46]. Figure 4 shows computed and experimental [47] dependences of the gas mixture combustion velocity V_f on mean velocity of turbulent pulsations V_{rms}; the mixture compositions were $CH_3OH + 1.8(O_2 + 1.6N_2)$ and $CH_3OH + 3(O_2 + 1.6N_2)$. Results are in good agreement.

Predetonation time t_d results in a hydrogen–air mixture with different volume contents of nitrogen C_{N_2} and the experimental data [45] are shown in Fig. 5. Calculations are in good agreement with experiments for nitrogen content $\geq 30\%$.

Results of the predetonation length calculation in a hydrogen–air mixture for various equivalence coefficients ϕ and initial temperature $T_0 = 300$ K are shown in Fig. 6 together with the corresponding experimental data [48]. Predetonation length L_d is represented in terms of a dimensionless value [48]

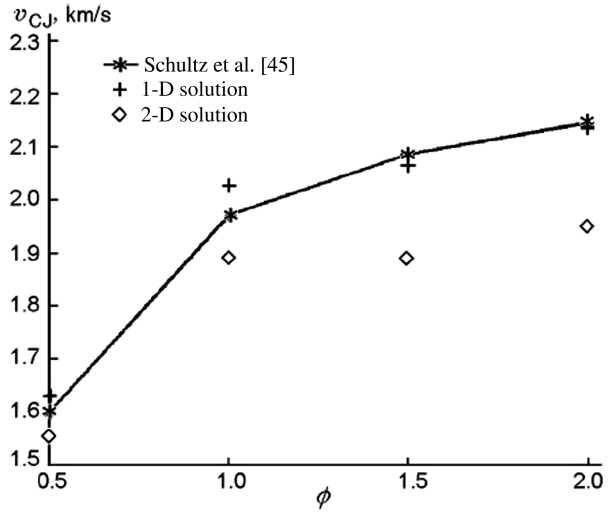

Fig. 3 Dependence of the CJ detonation velocity on the equivalence ratio ϕ. Theoretical and experimental [45] results.

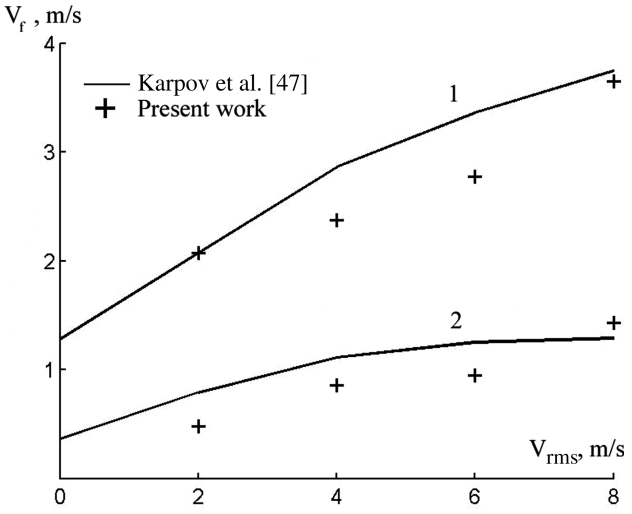

Fig. 4 Comparison of theoretical and experimental [47] results on the turbulent velocity of methyl alcohol combustion: V_f is flame velocity versus turbulent pulsations characteristic velocity V_{rms}. Curve 1: $CH_3OH + 1.8(O_2 + 1.6N_2)$; curve 2: $CH_3OH + 3(O_2 + 1.6N_2)$.

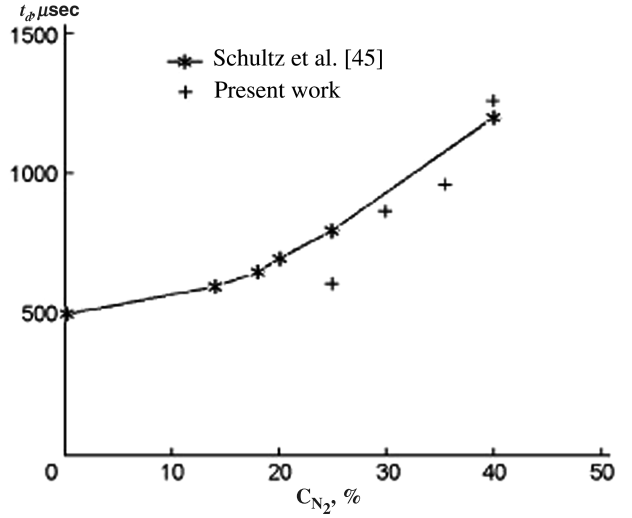

Fig. 5 Comparison of predetonation time theoretical and experimental [45] results for hydrogen–oxygen–nitrogen mixture (dependence on volumetric amount of nitrogen).

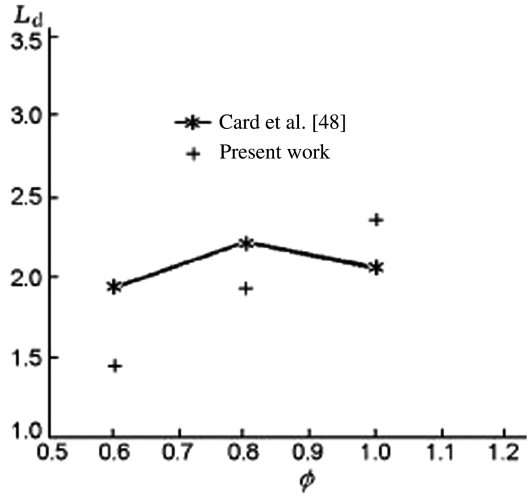

Fig. 6 Comparison of dimensionless predetonation length $\tilde{L}_d$ theoretical and experimental [48] results for hydrogen–air mixture (dependence on equivalence coefficient).

$$\tilde{L}_d = \left(\frac{L_d}{R}\right)\frac{10S_u}{a_p}(\sigma - 1)$$

where R is the tube radius, S_u is the laminar combustion velocity, a_p is the sound velocity at constant pressure in the combustion products, and σ is the ratio of gas densities before and after the reaction. The results are also in good agreement with the experimental data.

V. Evaluating Influence of Numerical Scheme Parameters

To verify the numerical scheme, shock wave simulations with an account of transport and turbulence models were processed. The shock wave propagation was studied for different parameters of the numerical scheme such as slope limiter and mesh size. We have tested the Zero limiter (the first-order accuracy scheme), the Minmod limiter (the second-order accuracy except for regions of sharp gradients of parameters), the van Leer symmetric limiter (the second-order accuracy), and the Superbee limiter (the second-order accuracy).

The following problem parameters were used to simulate the test problem: $p_0 = 1$ bar, $T_0 = 298$ K (the initial pressure and temperature), $p_{10} = 2$ bar (the elevated pressure), $k_0 = 0.01$ J/kg, $\nu_{T0} = 0.1$ cm^2/s (the initial turbulence energy and kinematic eddy viscosity), and the gas is nitrogen, $t_1 = 0.3$ ms.

The size of the domain was taken big enough to ensure that the shock wave does not reach the right end of the domain before $t = t_1$.

Figure 7 shows plots of eddy viscosity behind the propagating shock. With the increase of the limiter (from Zero to Superbee) the rate of the eddy viscosity jump behind the shock increases. It increases when we change to the second-order accuracy scheme (from Zero to Minmod); the difference between Minmod and van Leer results is small; the Superbee limiter brings small waves on the shape of the eddy viscosity profile; those waves are due to spurious velocity oscillations under this slope limiter. We conclude by using those results that the level of turbulent viscosity behind a shock does not depend on the slope limiter of the second-order scheme in case this scheme suppresses nonphysical oscillations of parameters.

The next set of calculations was used to estimate the influence of the numerical diffusion level. Because it is governed by the mesh size, we duplicated it. The results for the eddy viscosity rise behind the propagating shock are shown in Fig. 8. The change of the mesh size hardly influences the eddy viscosity behind a shock wave. An exception is the Superbee slope limiter which lowers oscillations in case of the larger mesh size. However, the difference is small in any case of the second-order accuracy scheme, though the level of numerical diffusion is duplicated. For the schemes of the first order of accuracy, the difference takes place, but it is still not high. Adequate schemes of the second order (Minmod and van Leer's limiters) do not manifest even a tiny difference for either mesh size.

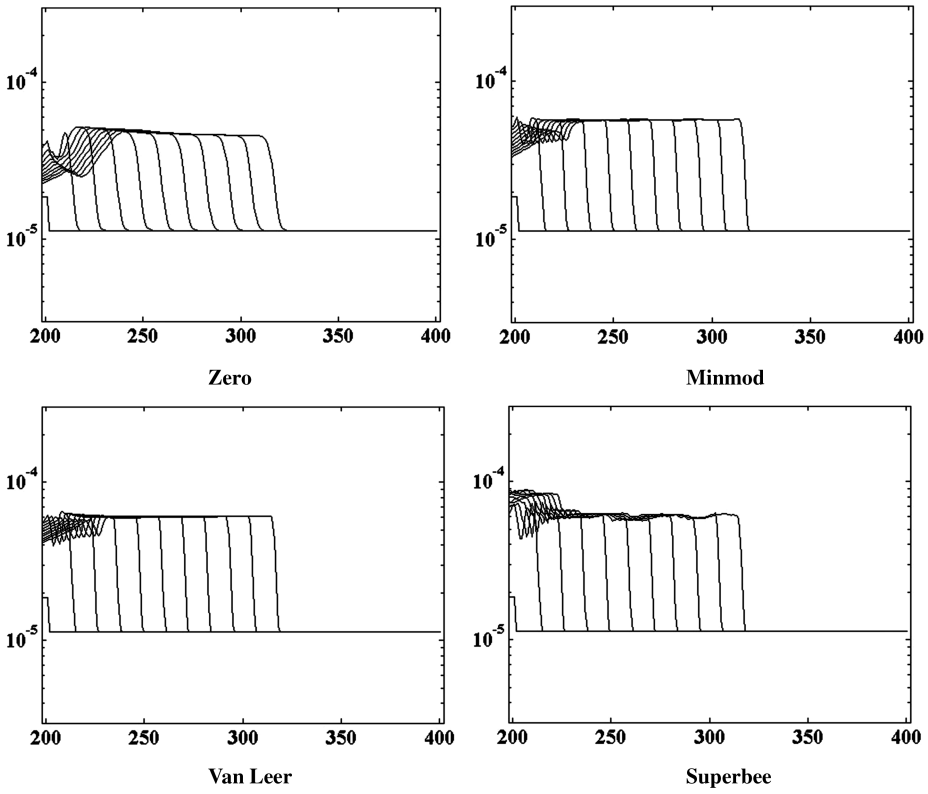

Fig. 7 Plots of dynamical eddy viscosity behind a propagating shock for four types of slope limiters. The vertical axis is logarithmic, and scaled in Pa · s; the horizontal axis shows numbers of grid nodes. Grid cell size is $\Delta x = 1$ mm.

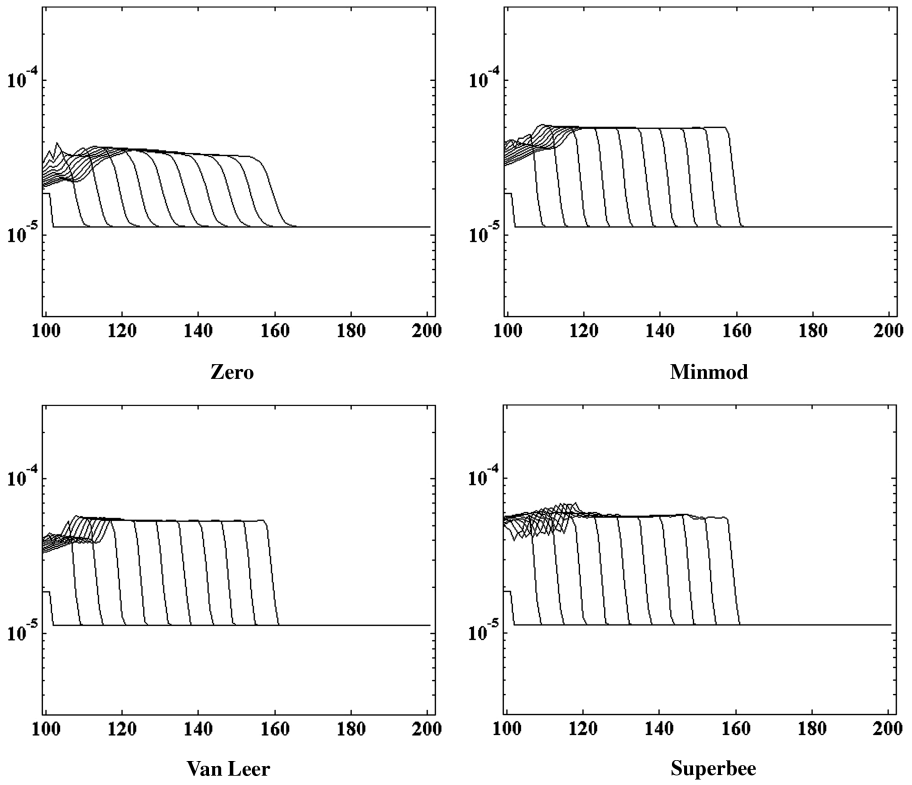

Fig. 8 Plots of eddy viscosity behind a propagating shock; the conditions are the same as shown in Fig. 7 but the mesh size is twice greater than $\Delta x = 2$ mm. Vertical axes are scaled in Pa · s; horizontal axes show numbers of grid nodes, which are twice less than on the previous plot.

Results obtained in this section come to the conclusion: in the case an adequate numerical scheme of the second order of accuracy in the regions of small gradients of parameters is chosen (adequacy means not producing significant spurious oscillations), then turbulent viscosity behind a propagating shock does not depend on the level of numerical diffusion. Thus, the last does not contaminate results for turbulent parameters in the vicinity of the shock. Based on these results, van Leer's limiter is chosen for the simulations in this paper.

The next series of calculations was aimed to study the influence of the mesh size on the parameters distribution in the detonation wave: von Neumann's pressure peak and species concentration. The detonation wave was initiated in a stoichiometric hydrogen–air mixture by a strong shock, and we studied its propagation for various mesh sizes. Parameters of the mixture were $p_0 = 1$ bar, $T_0 = 298$ K, and $e_{ig} = 1000$ kJ/kg. The length of the domain was 0.5 m. Figures 9a–9c show the results for different mesh sizes of $\Delta x = 2$ mm, 1 mm, and 0.5 mm, correspondingly.

The left-hand side Fig. 9 plots subsequent spatial distributions of pressure in the detonation wave demonstrating von Neumann's peak which lays within 18–21 bars obtained for the tested mixture. When the mesh size decreases, the pressure peaks increase slightly, and their thickness decreases. The right-hand side of Fig. 10 illustrates species volumetric shares C_k (in %) and temperature T (in K) shown on concentrations on the same plot. The left-hand Y axis of each plot corresponds to the volumetric share (scaled logarithmically), and the right-hand Y axis to the temperature (scaled linearly). To resolve the structure of the detonation wave more clearly, only 5 cm of the domain are shown on the right-hand plots. The nitrogen share is not illustrated because it is practically constant, and the other radical's concentrations are too small. The unburned gas is to the right of the detonation wave: it consists of hydrogen, oxygen, and nitrogen. When the detonation wave approaches, one can see the rapid increase of the radicals production in endothermic processes; the main chain branching reaction is $H_2 + O_2 \Rightarrow HO_2 + H$. The atomic hydrogen is then immediately involved into further chemical interactions producing other radicals, and finally water vapor. The perhydroxil HO_2 is consumed much slower. Temperature increase is small at this stage. After the radical's concentrations increase above some level, the water vapor production increases, and temperature grows rapidly. This decreases the radical's concentrations, except for C_{OH}, which is approaching a plateau from below: its remaining concentration is highest among the radicals. Other radicals, together with the initial species, approach their plateau from above. It is worth noticing that the remaining concentration of hydrogen is much higher than that of oxygen; thus, the stoichiometric mixture is not an optimal one. The remaining atomic hydrogen concentration is much higher than those of oxygen. The remaining volumetric share of perhydroxil is very low due to its poor stability at high temperatures. Thus, the thickness of the reaction zone could be effectively distinguished by the size of elevated perhydroxil concentration. The temperature possesses its maximal value when the radical's concentrations are approaching their plateau, and after that it decreases slightly.

When the mesh size is decreased, the thickness of the reaction zone decreases; however, it includes more computational cells. The qualitative and quantitative behaviors of the species concentrations and temperature are similar for the different mesh sizes.

VI. Calculations of Deflagration-to-Detonation Transition

The streamwise distributions of pressure and temperature on the axis of symmetry for $p_0 = 1$ bar and $T_0 = 295$ K, and different times, are plotted in Figs. 10a and 10b. An overdriven detonation wave is seen to form first in the deflagration-to-detonation transition (curve 4). Its velocity is higher than the CJ velocity, and a retonation wave starts propagating backward in the reaction products. The overdriven wave propagates gradually slowing down and weakening, with its pressure peak approaching the CJ pressure from above. The retonation wave fades swiftly, because the burned mixture produces no more energy release behind the wave to sustain it. Development of the combustion front velocity is shown in Fig. 11; the front position is defined as a location of maximal oxygen concentration gradient. It is seen from Fig. 11, that after the DDT, the front velocity exceeds the velocity of the CJ detonation (overdriven detonation), and then it gradually slows down to the CJ velocity.

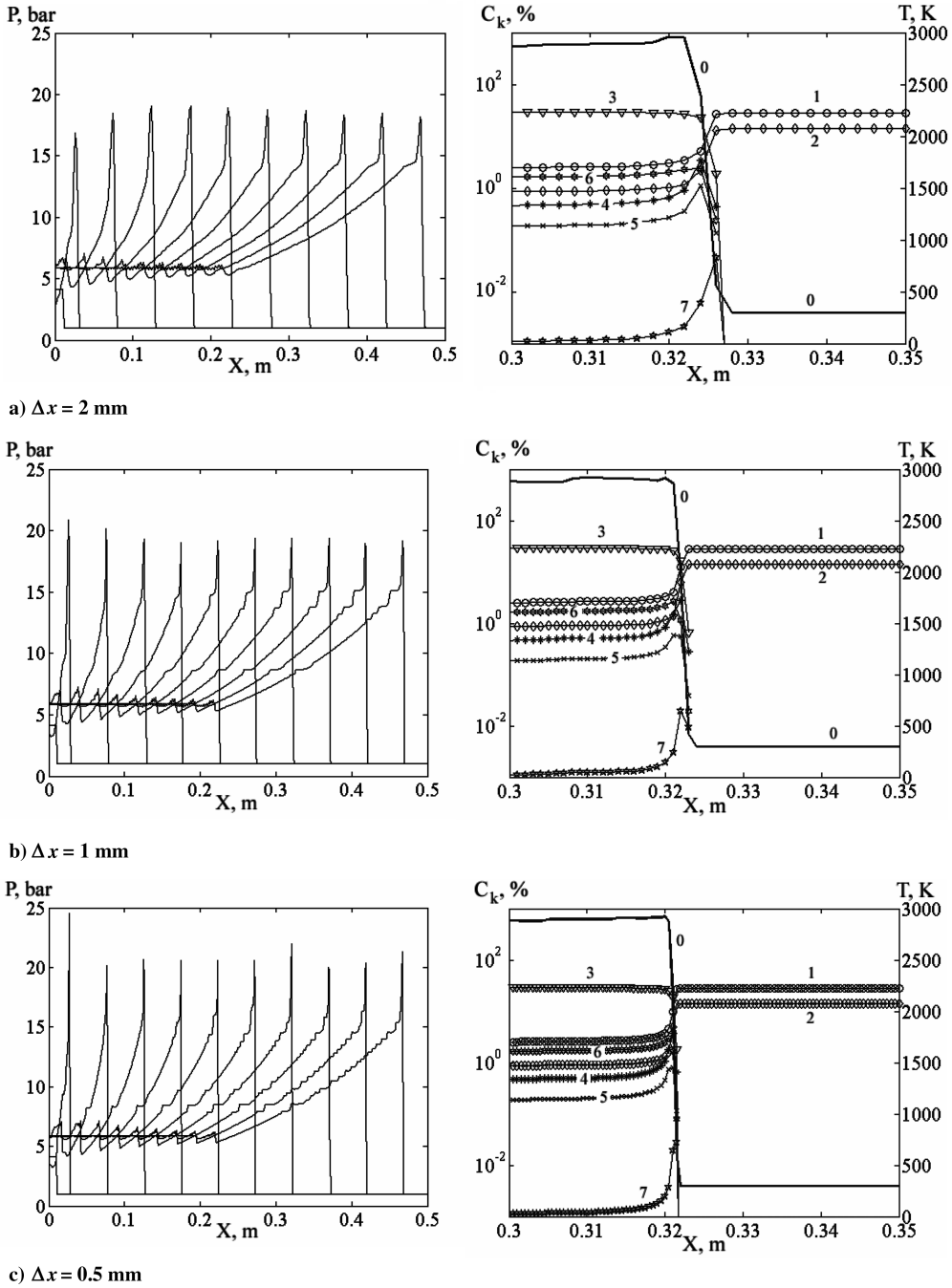

Fig. 9 Propagation of 1-D detonation wave, different mesh sizes. Pressure spatial distributions for subsequent times (left, scaled in bars); species volumetric shares (%) and temperature (Kelvin). Curves labeled 0: temperature, 1: C_{H_2}, 2: C_{O_2}, 3: C_{H_2O}, 4: C_H, 5: C_O, 6: C_{OH}, and 7: C_{HO_2}.

Numerical experiments performed for different initiation conditions help to explain why detonation forms on a contact surface between the flame front and the bow shock wave. The contact surface is formed due to the interaction of compression waves ahead of the flame zone, which catch each other because they propagate at a supersonic velocity with respect to the gas ahead, and at a subsonic velocity with respect to the gas behind. The gas portion between the leading shock and the contact surface has an elevated temperature. Therefore, the induction time is shorter there than in the portion between the contact surface and the flame front. The first thermal explosion takes place in the gas possessing an elevated temperature for maximal time, that is, in the layer neighboring the contact surface. This explosion ends in either detonation, or deflagration wave formation, which propagates in both directions from the exothermal center. The detonation wave is formed in the thermal explosion zone by the gradient mechanism, and it propagates in all directions from the self-ignition location. Intensity of retonation (backward detonation) drops rapidly when the wave enters the combustion products. The detonation wave overpasses the bow shock, and after that it propagates in a stagnant unburned medium. Even if it had propagated at a self-sustained mode with respect to the elevated gas parameters behind the leading shock wave, the interaction with the shock results in an overdriven detonation wave propagating into an undisturbed mixture, to a contact discontinuity and to a rarefaction continuous wave propagating backward. Velocity of the overdriven detonation gradually decreases down to the CJ wave velocity.

Turbulence influences the rate of localized chemical heat release after ignition and velocity of flame propagation, which in turn influences compression and shock waves formation ahead of the flame zone at the initial stage of the process. When strong shock waves are formed, the influence of turbulence on gas dynamics decreases, because the time scale of a shock is much smaller than that of the turbulence. However, our attempts to obtain the DDT numerically not using the turbulence model, and with the same kinetics and

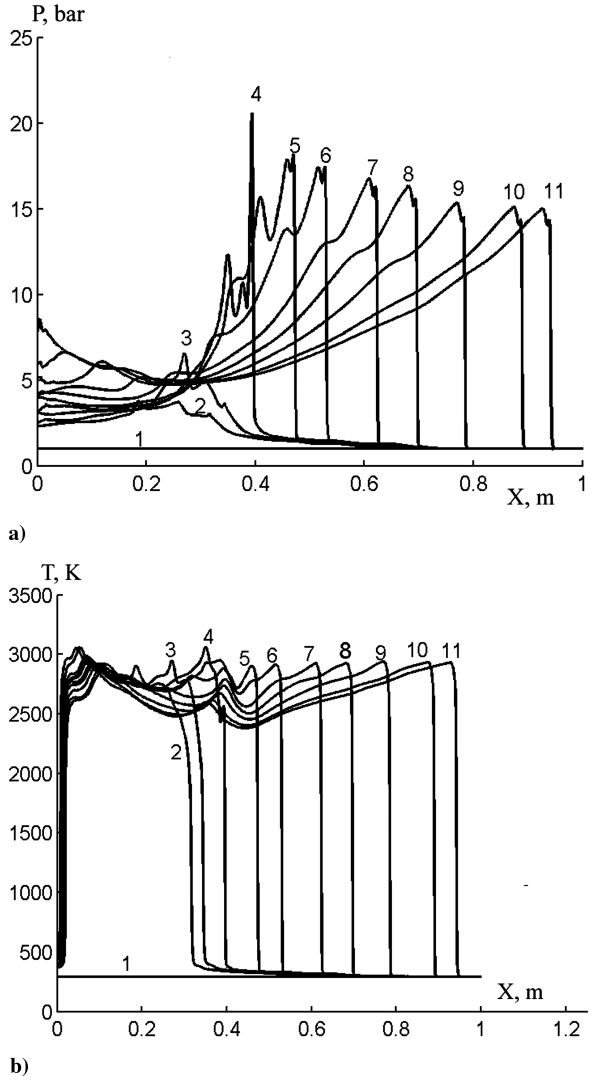

Fig. 10 a) Mean cross-section pressure profiles and b) temperature profiles computed for various time moments, hydrogen–air stoichiometric mixture. Curve number—time correspondence: 1: 0 ms, 2: 1.43 ms, 3: 1.48 ms, 4: 1.53 ms, 5: 1.56 ms, 6: 1.59 ms, 7: 1.64 ms, 8: 1.68 ms, 9: 1.73 ms, 10: 1.78 ms, and 11: 1.81 ms.

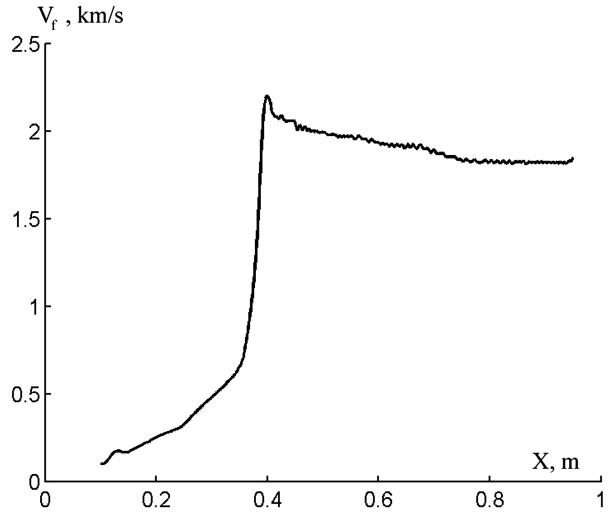

Fig. 11 Flame front velocity change along the tube, for hydrogen–air stoichiometric mixture combustion.

initiation condition, failed, because numerical diffusion was not sufficient to increase the transport processes up to the level providing effective flame acceleration. The onset of detonation could take place only for high initiation energies directly via initiation by a strong shock wave, and not by the DDT. This type of initiation was investigated in detail before [4,5].

A. Influence of Ignition Parameters, Initial Temperature, and Turbulent Energy on DDT

To study the influence of the ignition energy E_{ig} and time t_{ig}, and the initial turbulent energy and temperature on the DDT, a series of numerical experiments was performed.

It is convenient to continue the study in dimensionless parameters. The system of Eqs. (1–4), scaled to dimensionless form, includes the following criteria and dimensionless parameters of ignition:

$$\bar{t} = \frac{t}{t_{ref}}, \qquad \bar{x} = \frac{x}{x_{ref}}; \qquad Re = \frac{\rho_{ref}\sqrt{k_0}\ell_{ref}}{\eta_{ref}}, \qquad Sr = \frac{t_{ref}\sqrt{k_0}}{\ell_{ref}}$$

$$\bar{E}_{ig} = \frac{E_{ig}}{p_{ref}\ell_{ref}^3}, \qquad \bar{t}_{ig} = \frac{t_{ig}}{t_{ref}}, \qquad \bar{T}_0 = \frac{T_0}{T_{ref}}/$$

Here ℓ_{ref} is the integral scale of turbulence, k_0 is the initial turbulent energy, $\eta_{ref} = \eta(T_{ref}) + \eta_0^t$, $t_{ref} = 10^{-3}$ s, $T_{ref} = 300$ K, $p_{ref} = 1$ bar, $\rho_{ref} = p_{ref}/(R_{ref}T_{ref})$, and $R_{ref} = 335.94$ J/(kg K). The Reynolds and Strouhal numbers are based on the velocity of turbulent fluctuations. The increase of the Reynolds number characterizes the growth of turbulence in terms of the product of pulsation velocity and length scale. In this work, the following dimensionless parameters are varied: Reynolds number, Strouhal number, dimensionless ignition parameters, and dimensionless initial temperature.

Hereafter, all the parameters are assumed to be dimensionless, and we will drop tildes above their notations unless prompted in context.

Figure 12 shows dependence of predetonation length L_d on ignition energy E_{ig} in a tube with diameter 8 for the following cases: $Re = 2$ and $Sr = 0.013$; $Re = 4$ and $Sr = 0.130$; $t_{ig} = 0.01$ and $t_{ig} = 0.10$. The characteristic times are of the order of the acoustic time $t_{ac} = r_{ig}/a_p$; for the present ignition conditions it is equal to 0.03 dimensionless units (or 3×10^{-5} s). Plots in Fig. 11 show that the predetonation length first decreases with the increase of ignition energy, and then it is independent of it. When the ignition time decreases, the predetonation length decreases. This dependence is stronger at lower ignition energy. When initial turbulence energy increases ($Re = 4$, $Sr = 0.130$), the predetonation length decreases;

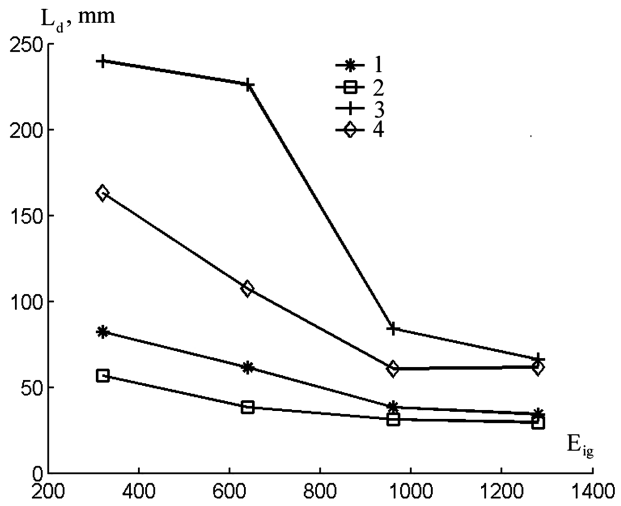

Fig. 12 Dependence of predetonation length on the ignition parameters and dimensionless ignition energy. Curves 1: $Re = 2$, $Sr = 0.013$, $t_{ig} = 0.01$; 2: $Re = 4$, $Sr = 0.130$, $t_{ig} = 0.01$; 3: $Re = 2$, $Sr = 0.013$, $t_{ig} = 0.10$; 4: $Re = 4$, $Sr = 0.130$, $t_{ig} = 0.10$. Dimensionless initial temperature $T_0 = 1$.

for higher ignition energy the decrease is less. The dimensionless length could be converted into dimensional ($x_{ref} = 0.005$ m).

The influence of the initial temperature on the DDT in gases is one of the least investigated features. The available experimental data are incomplete and often contradictory. For example, the increase of temperature in a stoichiometric hydrogen–oxygen mixture brought an increase of predetonation length [49]. For the diluted mixture, this dependence upon temperature was not distinguished [50]. Investigation of the DDT in hydrocarbon–air mixtures [11] showed that the predetonation length decreased when the initial temperature increased.

The reason for such contradictory results is that the increase of temperature brings opposite effects. On one hand, the chemical reaction rate grows with the temperature, therefore promoting the flame acceleration. On the other hand, the sound velocity in the unburned gas increases with temperature. This inhibits the DDT, because due to Zeldovich criterion [13,17,51,52], the transition to detonation is possible when the turbulent flame velocity reaches or surpasses the sonic velocity in the unburned gas. Probably, the influence of both effects brings about a variety of experimental results.

Figures 13–16 plot the dependence of predetonation length upon ignition energy for the following cases: $Re = 2$, and $Sr = 0.013$; $Re = 4$, and $Sr = 0.130$; for $t_{ig} = 0.01$ and $t_{ig} = 0.10$; and for initial temperatures $T_0 = 1.0$, $T_0 = 1.3$, and $T_0 = 1.7$. It is seen from those plots that:

1) For every tested case, and increase of the ignition energy release brought weaker dependence of the predetonation length upon the initial temperature. This result is explained that by increasing the ignition energy, the initiation of detonation takes place, not via the DDT, but due to a direct initiation by a strong shock wave. The latter scenario is almost independent of temperature.

2) If the ignition energy is small ($E_{ig} = 320$), the predetonation length decreases with the increase of initial temperature (Figs. 13–16). The result testifies that for small ignition energy the development of the process of flame acceleration formation of shock waves ahead of it is rather slow, and the negative effect of the increase of sound velocity in the unburned gas is dominating, thus retarding the "coupling" of gas dynamical and chemical processes [13,17].

3) If the ignition energy is relatively high ($E_{ig} = 640$), and the ignition time is small (high rate of energy release), the predetonation length decreases by increasing the initial temperature from 1.0 up to temperature 1.3; further increase of the initial temperature does not influence the predetonation length. The result shows that by increasing the ignition energy and the rate of its release a sufficient shock wave is formed ahead of the turbulent flame zone, and the initial velocity of the flame is fast enough to make the effect of sound

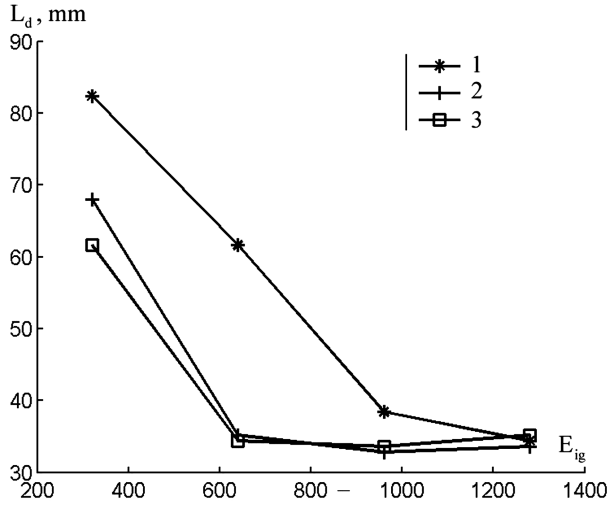

Fig. 13 Dependence of predetonation length on the dimensionless ignition energy for different initial temperatures. Results obtained for $Re = 2$, $Sr = 0.013$, and $t_{ig} = 0.01$. Curves 1: $T_0 = 1.0$; 2: $T_0 = 1.3$; 3: $T_0 = 1.7$.

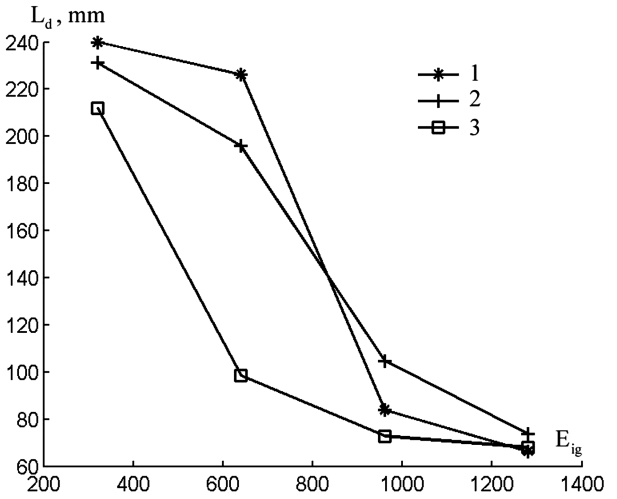

Fig. 14 Dependence of predetonation length on the dimensionless ignition energy for different initial temperatures obtained for $Re = 2$, $Sr = 0.013$, and $t_{ig} = 0.10$. Curves 1: $T_0 = 1.0$; 2: $T_0 = 1.3$; 3: $T_0 = 1.7$.

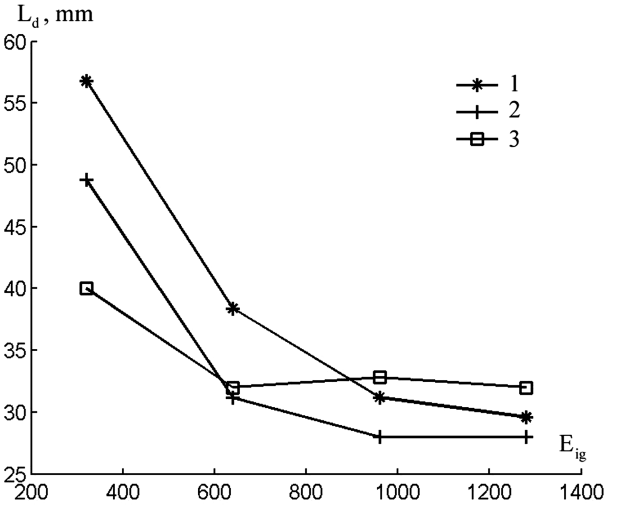

Fig. 15 Dependence of predetonation length on the dimensionless ignition energy for different initial temperatures obtained for $Re = 4$, $Sr = 0.130$, and $t_{ig} = 0.01$. Curves 1: $T_0 = 1.0$; 2: $T_0 = 1.3$; 3: $T_0 = 1.7$.

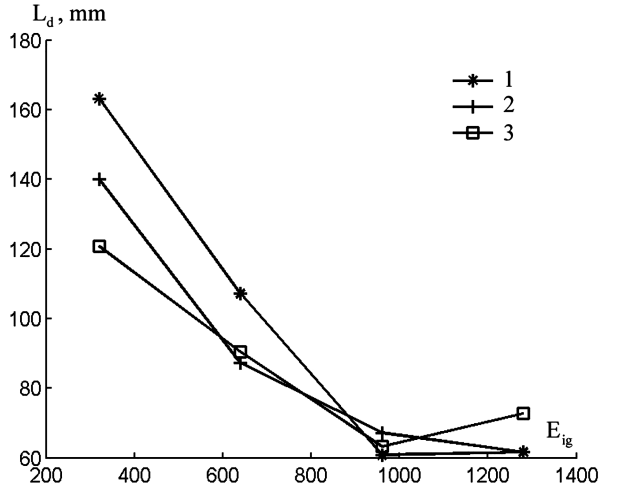

Fig. 16 Dependence of predetonation length on the dimensionless ignition energy for different initial temperatures obtained for $Re = 4$, $Sr = 0.130$, and $t_{ig} = 0.10$. Curves 1: $T_0 = 1.0$; 2: $T_0 = 1.3$; 3: $T_0 = 1.7$.

velocity increase negligible. In this case, the effect of chemical energy-release activation with an increase of temperature becomes dominating.

4) For higher ignition energy ($E_{ig} = 900, 1280$), a strong shock wave is formed, and the temperature increase behind the shock is sufficient to initiate chemical reactions. Turbulence almost does not influence the detonation initiation. The dependence predetonation length on temperature can be nonmonotonous. In general, the predetonation length is small, and final conclusions are questionable.

Figures 15 and 16 show that for low ignition energy, the Reynolds number increase brings about the decrease of predetonation length; for high ignition energy this dependence is not distinguished.

The decrease of the ignition time (Figs. 15 and 16) brings about the decrease of predetonation length both for low and high values of the ignition energy.

B. Influence of the Settling Chambers in the Ignition Section

To study the effect of the settling chambers (cavities) with an enlarged cross section on the detonation development, numerical modeling of the process was processed for a tunnel with a variable number of chambers shown in Fig. 1. Influence of the chambers number on the predetonation length and time was considered. The tube diameter was 8, the cavity diameter was 16, the cavity length was $L_c = 8$, and the bridge length between two cavities was $L_b = 3.0$. Ignition is performed in a ball-shaped volume in the center of the first cavity $r_{ig} = 2$. The ignition time $t_{ig} = 0.10$ is less than the acoustic time.

Figure 17 shows density distribution in a system with a four-chamber system for different times. The velocity vectors are shown as segments with various lengths and directions. The mapping colors palette is shown on the top of the figure. The darkest color corresponds to the lowest density, which characterizes burned reaction products heated by energy release in chemical reaction. The results are as follows.

The time moment $t = 0.42$ corresponds to the flame transfer from the first chamber to the second. The flame front does not reach the first chamber walls at this time. Low density distinguishes high temperature portion, which relates to the combustion products, while the density near the walls is still high due to compression of the unburned mixture.

At time $t = 0.82$ the flame front enters the third chamber. The pressure in the first and the second chambers becomes substantially increased owing to the fuel burnout. The gas velocity on the entrance of the fourth chamber increases.

By time moment $t = 1.01$ the flame front enters the fourth chamber. Pressure in the first three chambers now decreases slightly due to the burned gas expansion in the forward direction.

By the time moment $t = 1.25$ the flame front leaves the fourth chamber and enters the tunnel proper. Significant gas compression is distinguished ahead of the front (Fig. 17), which corresponds to a shock wave. Combustion does not yet begin in this shock wave.

At $t = 1.29$ the transition to detonation takes place. The pressure and temperature drastically increase on the shock wave; the spots of detonation initiation are near the tube wall. The velocity field (Fig. 17) demonstrates the divergence of gas in both directions from the transition site.

The time moment $t = 1.33$ corresponds to the detonation wave propagating in the unburned gas. It is seen also that some remaining fuel is still burning near the walls of the chambers: the gas density near the walls still remains high, which for an almost uniform pressure inside chamber corresponds to much lower temperature near the walls.

To study the influence of the settling chambers number on the predetonation length and time, we changed the number of chambers from zero to five.

Figures 18 and 19 show dependencies of predetonation length and time on the settling chambers number N_c. Results were obtained for the following parameters: $\phi = 1$, $T_0 = 1.0$, $E_{ig} = 640$, $t_{ig} = 0.01$, $Re = 4$, $Sr = 0.05$, $L_c = 8$, and $L_b = 3.2$. Figures 20 and 21 show development of the reaction front velocity (scaled by the sonic velocity at the initial state) and the turbulence energy in the reaction front along the tube k_f scaled by the initial energy of turbulence. Each curve on Figs. 20 and 21 is labeled with the chambers number. Figures 20b and 21b illustrate the process in the initial part of the tube.

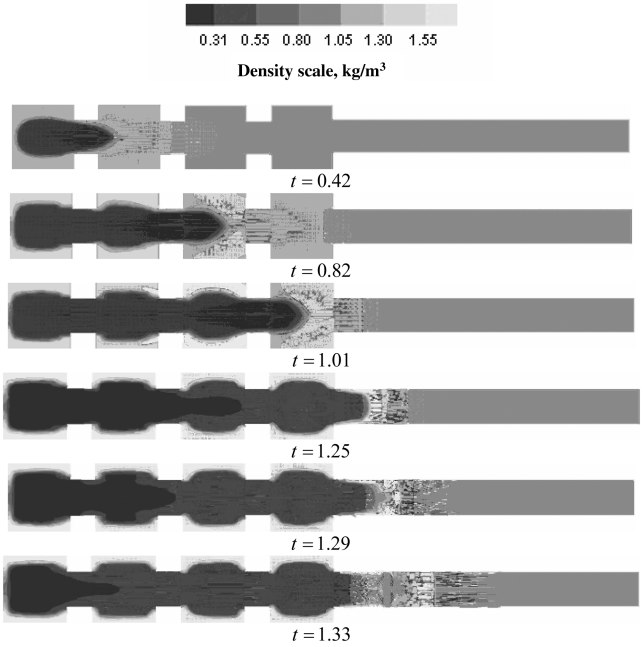

Fig. 17 Distribution of density and velocity in a four-chamber tube for different dimensionless times.

Both predetonation length and time decrease in the two-chamber system. However, presence of the third chamber brings a very small effect on those parameters. The third chamber brings a high increase of turbulence energy, but after the reaction front passes this chamber, the turbulence energy level drops down to those of the two-chamber system (Fig. 21).

Presence of the fourth chamber decreases predetonation length and time significantly. Both the turbulence energy and the flame front velocity are increased, thus the DDT is promoted (Fig. 20.)

Presence of the fifth chamber brings an insufficient influence on predetonation length and time. The flame front velocity decreases at the entrance of the fifth chamber, and the transition to detonation takes place only at the exit of the chamber.

The temporal evolution of turbulent kinetic energy in the tube containing four settling cavities in the ignition section is shown in Fig. 22, which shows that the increase of turbulent kinetic energy takes place in a vortex after the flow passes a bridge between cavities;

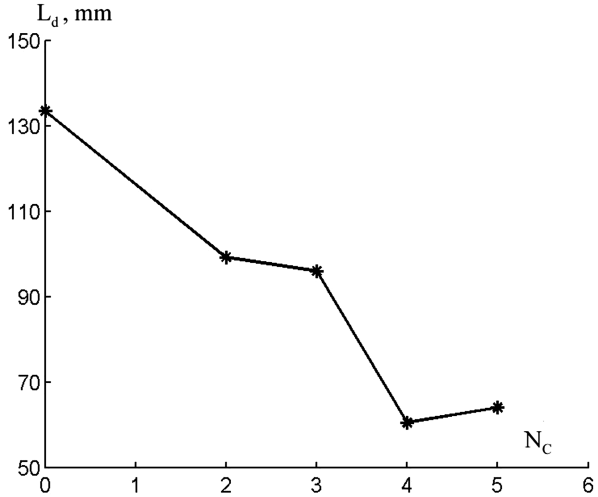

Fig. 18 Dependence of predetonation length on the number of settling cavities N_c.

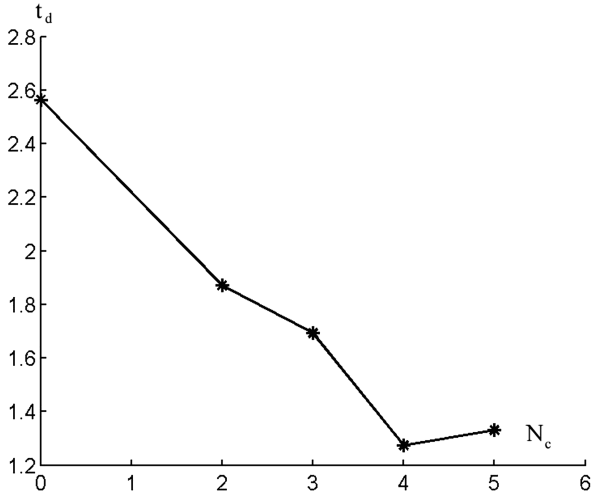

Fig. 19 Dependence of dimensionless predetonation time on the number of cavities N_c.

the maximal increase of the turbulence energy takes place in the third cavity.

Figure 20 shows that the increase of the number of settling chambers brings the growth of the amplitude of the flame front pulsations. Those pulsations are determined by the flame velocity increase as it transfers from one chamber to another via a narrow bridge tube and the flame front velocity deceleration as it enters a new chamber. The amplitude of those pulsations rises with the number of chambers until it reaches a constant value, and the mean flame front velocity rises from chamber to chamber until reaching a quasi-steady mode. From this point of view, it is worthwhile to compare curves 4 and 5 in Fig. 20b. After the flame leaves the fourth chamber, its velocity is high enough to launch the transition to detonation. But the presence of the fifth chamber brings deceleration of the flame front; therefore the DDT takes place only when the flame leaves the fifth chamber, and thus the predetonation time consequently increases. We come to the conclusion that the optimal chambers number, for the configuration considered, is equal to 4.

The theoretical explanation is based on the necessity condition of the DDT, namely, the so-called coupling of the gas dynamic processes (the generation and propagation of compression waves in unburned gas) with the chemical kinetics and other processes determining the flame front propagation [12,16,51,52]. This condition is the flame front velocity exceeding the sonic velocity in undisturbed gas, where the wave complex propagates, including the combustion front and compression waves ahead of it. The analysis of the results has shown that a piston effect of the combustion products expanding in cavities brings a sharp growth of the flame velocity at the entrance of a narrow tube. After the flame enters a new chamber, its velocity decreases, but increasing flow turbulization brings its new acceleration to the exit of the chamber. On the exit of the fourth

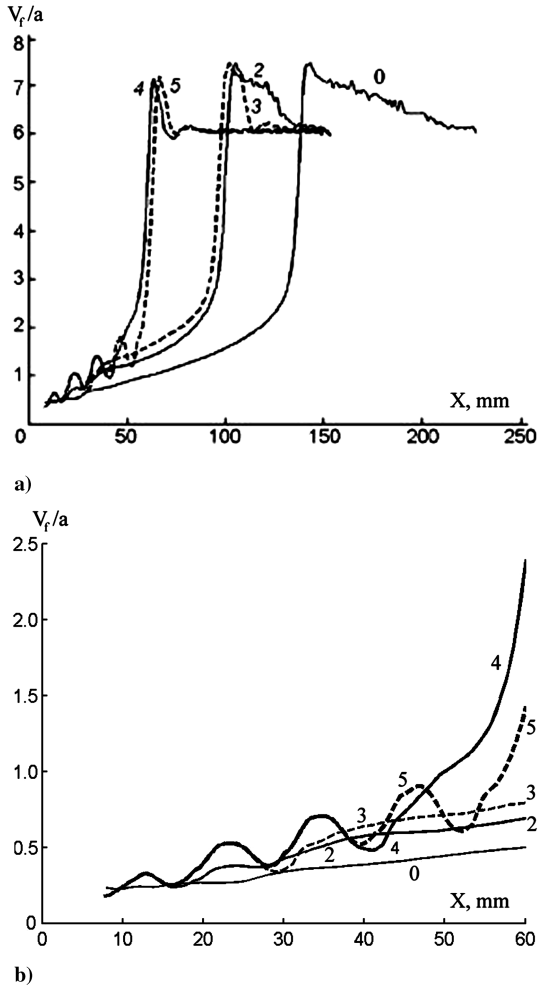

Fig. 20 Dimensionless flame front velocity along the tube, for a different number of settling chambers in the initial part of the tube: a) full length, b) initial section. Curves are labeled with the number of chambers.

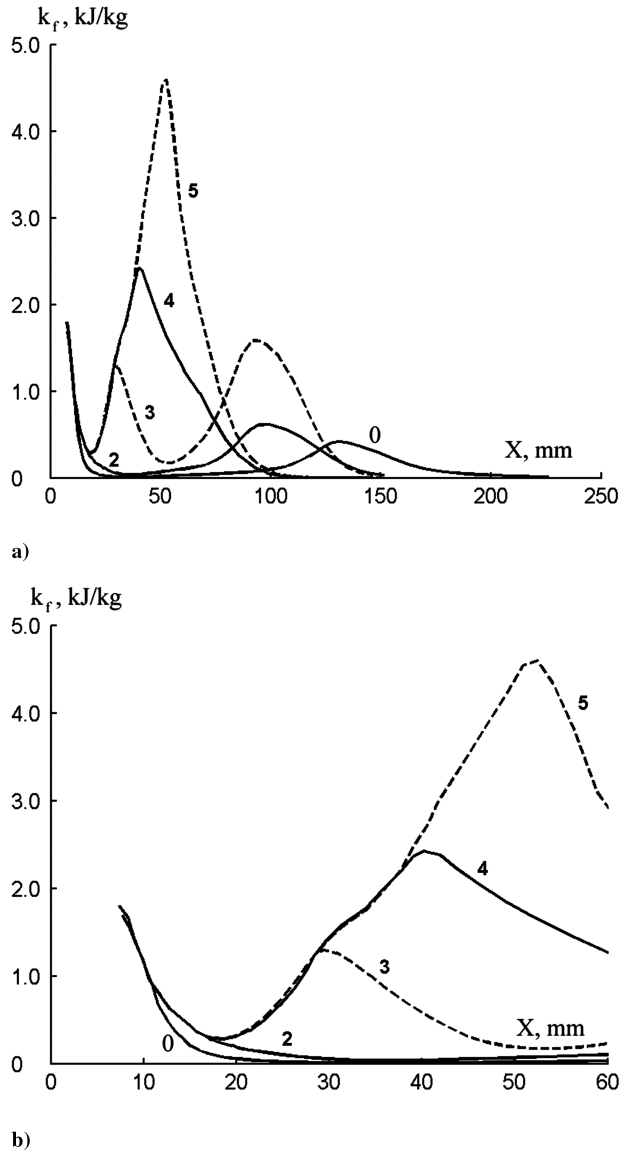

Fig. 21 Turbulent energy k_f at the reaction front, for various number of settling chambers: a) full length, b) initial section. Curves are labeled with the number of chambers.

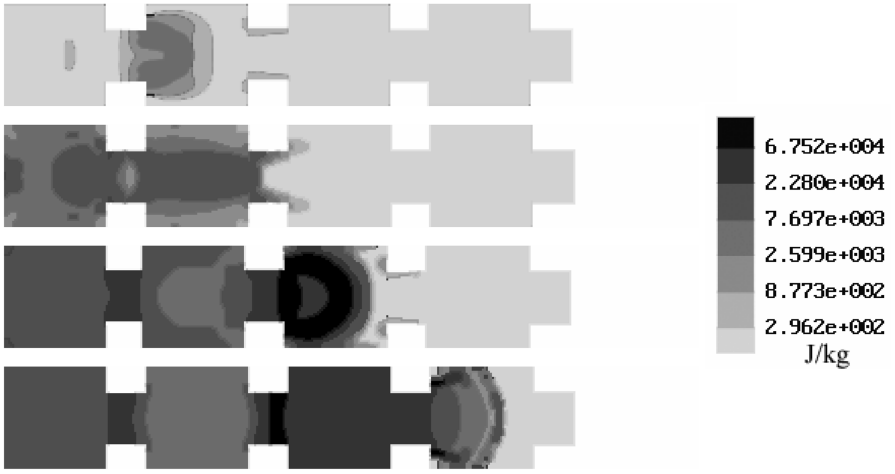

Fig. 22 Temporal evolution of the kinetic energy of turbulence in the tube with four cavities in the ignition section.

chamber, the flame velocity is significantly higher than those needed in the criterion. Therefore, further increase of the number of settling chambers does not promote the DDT but brings an increase of both predetonation length and time.

This result was obtained for a certain fuel mixture and device geometry. If the governing parameters change, another number of chambers could be optimal. For example, the study of the DDT in the tubes of different dimensions and with different fuel has shown that the configuration for the shortest predetonation length and time could contain two chambers [53,54].

VII. Conclusions

The investigation results show that in the process of the DDT, the detonation initiation takes place in local exothermal centers (hot spots) between the accelerating combustion zone and the leading shock. Those hot spots are the result of the flow inhomogeneity; they originate mostly on contact surfaces which are results of shock wave interaction.

The hot spots are either sources of deflagration, or detonation waves, depending on their structure. If the detonation wave originates, it propagates in all the directions from the source, it overpasses the leading bow shock, and after this interaction a quasi-flat overdriven detonation wave propagates in the unburned mixture. The velocity of this wave gradually decreases down to the velocity of CJ self-sustaining detonation.

If a deflagration wave originates in the hot spot, it propagates with much slower velocity. It gives time to ignite the other hot spots, and, finally, the process can also bring a detonation wave origination.

The predetonation length and time decrease with the increase of ignition energy, turbulent Reynolds number of the flow, and with the decrease of ignition time. Dependence of those characteristics on the Reynolds number and the ignition time is stronger at lower ignition energy, and becomes weaker at higher ignition energy release.

The presence of several settling chambers with wider cross section in the ignition portion of the system brings a shortening of the predetonation length and stabilizes the DDT.

Increasing the number of the settling chambers promotes the DDT whereas the velocity of turbulent flame at the exit of the last chamber is subsonic. Further increase does not promote the DDT and even delays it in the case of a high cross-section ratio.

Increase of the initial temperature of the mixture brings either shortening, or a prolongation of predetonation length and time, depending on the ignition energy and geometry of the device.

Acknowledgment

The Russian Foundation for Basic Research (Grant 08-03-00190) is acknowledged for support of this work.

References

[1] Bishimov, E., Korobeinikov, V. P., Levin, V. A., and Cherny, G. G., "One Dimensional Unsteady Flows of a Combustible Gas Mixture Allowing for Finite Chemical Reaction Rates," *Fluid Dynamics*, Vol. 3, No. 6, 1972, pp. 1–8. doi:10.1007/BF01022864

[2] Cherny, G. G., *Supersonic Flow with Combustion and Detonation Fronts*, Science Publishers, Moscow, 1969, pp. 561–578 (in Russian).

[3] Larin, O. B., and Levin, V. A., "Investigation of Detonation Wave of Double Front Structure Attenuation," *Proceedings of the Academy of Sciences of the USSR, Physical Cehmistry Section*, No. 3, 1971, pp. 59–65 (in Russian).

[4] Levin, V. A., and Markov, V. V., "Initiation of Detonation by Concentrated Release of Energy," *Combustion, Explosion and Shock Waves*, Vol. 11, No. 4, 1975, pp. 623–629.

[5] Levin, V. A., Markov, V. V., and Osinkin, S. F., "Direct Initiation of Detonation in a Hydrogen–Oxygen Mixture Diluted with Nitrogen," *Fluid Dynamics*, Vol. 27, No. 6, 1993, pp. 873–876. doi:10.1007/BF01051365

[6] Clarke, J. F., Kassoy, D. R., and Riley, N., "On the Direct Initiation of a Plane Detonation Wave," *Proceedings of the Royal Society of London, Series A: Mathematical and Physical Sciences*, Vol. 408, 1986, pp. 129–148. doi:10.1098/rspa.1986.0113

[7] Oppenheim, A. K., and Urtiew, P. A., "Experimental Observations of the Transition to Detonation in an Explosive Gas," *Proceedings of the Royal Society of London, Series A: Mathematical and Physical Sciences*, Vol. 295, 1966, pp. 13–28. doi:10.1098/rspa.1966.0223

[8] Salamandra, G. D., "On the Interaction of a Flame with a Shock Wave," *Physical Gas Dynamics*, USSR Academy of Sciences Publishers, Moscow, 1959, pp. 163–167 (in Russian).

[9] Bazhenova, T. V., and Soloukhin, R. I., "Gas Ignition Behind the Shock Waves," *Proceedings of the 7th International Symposium on Combustion*, Butterworths, London, 1959, pp. 866–875.

[10] Soloukhin, R. I., *Methods of Measuring and Main Results of Experiments in Shock Tubes*, Novosibirsk State University Publishers, Novosibirsk, Russia, 1969 (in Russian).

[11] Smirnov, N. N., and Boichenko, A. P., "Transition of Combustion to Detonation in Gasoline-Air Mixtures," *Combustion, Explosion and Shock Waves*, Vol. 22, No. 2, 1986, pp. 187–190. doi:10.1007/BF00749265

[12] Smirnov, N. N., and Tyurnikov, M. V., "Experimental Investigation of Deflagration to Detonation Transition in Hydrocarbon-Air Gaseous Mixtures," *Combustion and Flame*, Vol. 100, No. 4, 1995, pp. 661–668. doi:10.1016/0010-2180(94)00151-H

[13] Zeldovich, Y. B., Librovich, V. B., Makhviladze, G. M., and Sivashinsky, G. I., "On the Onset of Detonation in a Non-Uniformly Pre-Heated Gas," *Journal of Applied Mechanics and Technical Physics*, Vol. 11, No. 2, 1970, pp. 264–270.

[14] Merzhanov, A. G., "On Critical Conditions for Thermal Explosion of a Hot Spot," *Combustion and Flame*, Vol. 10, No. 4, 1966, pp. 341–348. doi:10.1016/0010-2180(66)90041-1

[15] Borisov, A. A., "On the Origin of the Exothermic Centers in Gaseous

Mixtures," *Acta Astronautica*, Vol. 1, Nos. 7–8, 1974, pp. 909–920. doi:10.1016/0094-5765(74)90059-9

[16] Kailasanath, K., and Oran, E. S., "Ignition of Flamelets Behind Incident Shock Waves and the Transition to Detonation," *Combustion Science and Technology*, Vol. 34, No. 1, 1983, pp. 345–362. doi:10.1080/00102208308923699

[17] Zeldovich, Y. B., Gelfand, B. E., Tsyganov, S. A., Frolov, S. M., and Polenov, A. N., "Concentration and Temperature Non-Uniformities of Combustible Mixture as a Reason of Pressure Waves Generation," *Dynamics of Explosions*, edited by A. Kuhl, and A. K. Oppenheim, AIAA, New York, Vol. 114, 1988, p. 99.

[18] Smirnov, N. N., Demyanov, A. Y., and Panfilov, I. I., "Deflagration to Detonation Transition," *Chemical Physics of Combustion and Explosion: Detonation*, USSR Acad. Sci. Publ., Chernogolovka, 1989, pp. 52–56 (in Russian).

[19] Frolov, S. M., "The Effect of Non-Ideality on the Explosion Origin and Propagation," Ph.D. Dissertation, N. N. Semenov Institute of Chemical Physics, Moscow, 1992 (in Russian).

[20] Smirnov, N. N., Nikitin, V. F., Boichenko, A. P., Tyurnikov, M. V., and Baskakov, V. V., "Deflagration to Detonation Transition in Gases and its Application to Pulse Detonation Devices," *Gaseous and Heterogeneous Detonations: Science to Applications*, edited by G. D. Roy, S. Frolov, K. Kailasanath, and N. Smirnov, ENAS Publishers, Moscow, 1999, pp. 65–94.

[21] Gostintsev, Y. A., Istratov, A. G., and Fortov, V. E., "On Fractal Structure of Turbulent Spherical Flame," *Russian Academy of Sciences*, Vol. 353, No. 1, 1997, pp. 55–57 (in Russian).

[22] Gostintsev, Y. A., Istratov, A. G., Kidin, N. I., and Fortov, V. E., "Autoturbulization of Gas Flames: Analysis of Experimental Results," *Thermophysics of High Temperatures*, Vol. 37, No. 2, 1999, pp. 306–312 (in Russian).

[23] Gostintsev, Y. A., Istratov, A. G., Kidin, N. I., and Fortov, V. E., *Thermophysics of High Temperatures*, Vol. 37, No. 2, 1999, pp. 633–637 (in Russian).

[24] Adushkin, V. V., Fortov, V. E., Gostintsev, Y. A., Istratov, A. G., Karpov, V. P., Kidin, N. I., Fedorov, A. V., and Shatskikh, Y. V., "Development of Instability in Spherical Gaseous Flames and Origin of Detonation," *Proceedings of the 13th Symposium on Combustion and Flame on Disc* [CD-ROM], Chernogolovka, Moscow Region, 7–11 Feb. 2005.

[25] Brown, C. J., and Thomas, G. O., "Experimental Studies of Shock-Induced Ignition and Transition to Detonation in Ethylene and Propane Mixtures," *Combustion and Flame*, Vol. 117, No. 4, 1999, pp. 861–870. doi:10.1016/S0010-2180(98)00133-3

[26] Khohlov, A. M., and Oran, E. S., "Numerical Simulation of Detonation Initiation in a Flame Brush: The Role of Hot Spots," *Combustion and Flame*, Vol. 119, No. 4, 1999, pp. 400–416. doi:10.1016/S0010-2180(99)00058-9

[27] Shchelkin, K. I., and Troshin, Y. K., *Gas Dynamics of Combustion*, USSR Academy of Sciences Publishes, Moscow, 1963 (in Russian).

[28] Knystautas, R., Lee, J. H. S., Shepherd, J. E., and Teodorczyk, A., "Flame Acceleration and Transition to Detonation in Benzene—Air Mixtures," *Combustion and Flame*, Vol. 115, No. 3, 1998, pp. 424–436. doi:10.1016/S0010-2180(98)00014-5

[29] Abdullin, R. H., Babkin, V. S., Borisenko, A. V., and Senachin, P. K., *Combustion of Gas in a Linear System of Connected Vessels*, Preprint of Altay Technological University, Barnaul, Russia, 1997, pp. 3–55 (in Russian).

[30] Azatyan, V. V., "The Role of Chain Branching Mechanism in Ignition and Combustion of Hydrogen-Oxygen Mixtures Near the Third Limit," *Kinetics and Catalysis*, Vol. 37, No. 4, 1996, pp. 512–520.

[31] Ivashnyov, O. E., and Smirnov, N. N., "Shock Rarefaction Waves in Unstable Boiling Liquid," *Proceedings of Russian Academy of Sciences, Fluid Dynamics*, Vol. 35, No. 4, 2000, pp. 20–33 (in Russian).

[32] Ivashnyov, O. E., Ivashneva, M. N., and Smirnov, N. N., "Slow Waves of Boiling Under Hot Water Depressurisation," *Journal of Fluid Mechanics*, Vol. 413, June 2000, pp. 149–180. doi:10.1017/S0022112000008417

[33] Smirnov, N. N., and Nikitin, V. F., "The Influence of Confinement Geometry on Deflagration to Detonation Transition in Gases," *Journal of Physics IV France*, Vol. 12, No. 7, 2002, pp. 341–351.

[34] Smirnov, N. N., and Panfilov, I. I., "Deflagration to Detonation Transition in Combustible Gas Mixtures," *Combustion and Flame*, Vol. 101, Nos. 1–2, 1995, pp. 91–100. doi:10.1016/0010-2180(94)00190-4

[35] Smirnov, N. N., Nikitin, V. F., Tyurnikov, M. V., Boichenko, A. P., Legros, J. C., and Shevtsova, V. M., "Control of Detonation Onset in Combustible Gases," *High Speed Deflagration and Detonation*, edited by G. D. Roy, S. Frolov, D. Netzer, and A. Borisov, Elex-KM Publishers, Moscow, 2001, pp. 3–30.

[36] Hamming, R. W., *Numerical Methods for Scientists and Engineers*, McGraw–Hill, New York, 1962.

[37] Philip, M., "Experimentelle und Theoretische Untersuchungen zum Stabilitatsverhalten von Drallflammen mit Zentraler Ruckstromzone," Ph.D. Dissertation, Karlsruhe University, Germany, 1991 (in German).

[38] Starik, A. M., and Titova, N. S., "Initiation of Detonation in a Supersonic Flow Behind a Shock Wave Under Non-Equilibrium Excitation of Vibrational Degrees of Freedom of Molecules," *Gaseous and Heterogeneous Detonations*, edited by G. D. Roy, S. Frolov, K. Kailasanath, and N. Smirnov, ENAS Publishers, Moscow, 1999, pp. 225–240.

[39] Pironneau, O., and Mohammadi B., *Analysis of the K-Epsilon Turbulence Model*, Mason Editeur, Paris, 1994.

[40] Oran, E. S., and Boris J. P., *Numerical Simulation of Reactive Flow*, Elsevier, New York. 1987.

[41] Smirnov, N. N., and Nikitin, V. F., "Unsteady-State Turbulent Diffusive Combustion in Confined Volumes," *Combustion and Flame*, Vol. 111, No. 3, 1997, pp. 222–256. doi:10.1016/S0010-2180(97)80786-9

[42] Anderson, D. A., Tannehill, J. C., and Pletcher, R. H., *Computational Fluid Mechanics and Heat Transfer*, Hemisphere, New York, 1984.

[43] van Leer, B., "Towards the Ultimate Conservative Difference Scheme. 2: Monotonicity and Conservation Combined in a Second Order Scheme," *Journal of Computational Physics*, Vol. 14, No. 4, 1974, pp. 361–370. doi:10.1016/0021-9991(74)90019-9

[44] van Leer, B., "Towards the Ultimate Conservative Difference Scheme. 3: Upstream-Centered Finite-Difference Schemes for Ideal Compressible Flow," *Journal of Computational Physics*, Vol. 23, No. 3, 1977, pp. 263–275. doi:10.1016/0021-9991(77)90094-8

[45] Schultz, E., Wintenberger, E., and Shepherd, J., "Investigation of Deflagration to Detonation Transition for Application to Pulse Detonation Engine Ignition Systems," *16th JANNAF Propulsion Meeting*, AIAA, Reston, VA, 1999.

[46] Smirnov, N. N., and Nikitin, V. F., "Influence of Channel Geometry and Mixture Temperature on Deflagration to Detonation Transition in Gases," *Combustion, Explosion and Shock Waves*, Vol. 40, No. 2, 2004, pp. 186–199. doi:10.1023/B:CESW.0000020141.67981.5f

[47] Karpov, V. P., Politenkova, G. G., and Severin, E. S., "Turbulent Combustion of Alcohols," *Combustion, Explosion and Shock Waves*, Vol. 22, No. 4, 1986, pp. 397–399.

[48] Card, J., Rival, D., Ciccarelli, G., Murray, S., and Zhang, F., "DDT in Fuel-Air Mixtures at Elevated Temperatures and Pressures," *Proceedings of the 18th International Colloquium on the Dynamics of Explosions and Reactive System*, University of Washington, Seattle, WA, 2001.

[49] Laffitte, P., "Influence of Temperature on the Formation of Explosive Waves," *Comptes Rendus de l'Academie des Sciences, Paris*, Vol. 186, No. 5, 1928, p. 951.

[50] Bollinger, L. E., Fong, M. C., and Edse, R., "Experimental Measurements and Theoretical Analysis of Detonation Induction Distance," *ARS Journal*, Vol. 31, No. 5, 1961, p. 588.

[51] Cheng, R. K., Short, J. M., and Oppenheim, A. K., "Diagnostics of the Exothermic Process," *Experimental Diagnostics in Gas Phase Combustion System*, edited by B. T. Zinn, Vol. 53, Progress in Astronautics and Aeronautics, AIAA, New York, 1977, pp. 611–627.

[52] Dold, J. W., and Short, M., "Compressibility Corrections to Zeldovich's Spontaneous Flame and the Onset of an Explosion in a Non-Uniformly Pre-Heated Medium," *Proceedings of the 13th ICDERS*, Nagoya University, Nagoya, 1991, p. 63.

[53] Smirnov, N. N., Nikitin, V. F., Alyari-Shourekhdeli, Sh., Shevtsova, V. M., and Legros, J. C., "Onset of Detonation in Pulse Detonating Devices," *Proceedings of the 17th ONR Propulsion Meeting*, edited by G. D. Roy, and A. Ghoneim, MIT, Cambridge, MA, 2004, pp. 161–167.

[54] Smirnov, N. N., Nikitin, V. F., Alyari-Shourekhdeli, Sh., and Legros, J. C., "Deflagration to Detonation Transition in Gases: Scenario and Models," *Zeldovich Memorial International Conference on Combustion and Detonation*, Torus Press, Moscow, 30 Aug.–3 Sept. 2004, OP 25.

J. Powers
Associate Editor